

NEHRP Final Technical Report

USGS Award Number: G09AP00043

Title of award: Late Holocene Tectonics of Northwesternmost Washington: Laying the Groundwork for an Improved Model of Northern Cascadia Forearc Deformation: Collaborative Research with Humboldt State University and U.S. Geological Survey

Authors and affiliations:

Harvey M. Kelsey
Dept. of Geology
Humboldt State University
Arcata, CA 95521
707 826 3991; fax 707 826 5241
hmk1@humboldt.edu

Brian L. Sherrod
U. S. Geological Survey
Dept of Earth and Space Sciences, Box 351310
University of Washington
Seattle WA 98195
206 553-0153
bsherrod@ess.washington.edu

Richard J. Blakely
U. S. Geological Survey
345 Middlefield Road
Menlo Park, CA 94025
blakely@usgs.gov
650 329-5316

Thomas L. Pratt
U. S. Geological Survey
Dept of Earth and Space Sciences, Box 351310
University of Washington
Seattle WA 98195
tpratt@ocean.washington.edu
206 543-7358

Ralph A. Haugerud
U. S. Geological Survey
Dept of Earth and Space Sciences, Box 351310
University of Washington
Seattle WA 98195
rhaugerud@usgs.gov
206 713-7453

Award Period: 6/01/2009 through 5/31/2010

TITLE OF FINAL TECHNICAL REPORT:

Active faulting in the Bellingham forearc basin: north-south shortening at the northern end of the Cascadia subduction zone

Kelsey, H. M., Department of Geology, Humboldt State University, Arcata CA 95521

Sherrod, B. L., U. S. Geological Survey, University of Washington, Box 351310, Seattle WA 98195

Blakely, R. J., U. S. Geological Survey, 345 Middlefield Road, Menlo Park, CA 94025

Pratt, T. L., U. S. Geological Survey, University of Washington, Box 351310, Seattle WA 98195

Haugerud, R. A., U. S. Geological Survey, University of Washington, Box 351310, Seattle WA 98195

1. ABSTRACT

On the basis of residual gravity data, and supplemented by aeromagnetic data, the northern end of the actively deforming northern Cascadia forearc is at the latitude of the U. S.-Canadian border. We propose that the Bellingham Basin is the northern of four actively deforming basins that provide the structural context for deformation within the northern Cascadia forearc. The northern margin of the Bellingham Basin is defined by a set of Holocene-active faults identified for the first time in this paper. These faults, Drayton Harbor, Birch Bay, and Sandy Point, can be traced from onshore to offshore using a combination of aeromagnetic interpretation, analysis of LiDAR imagery, paleoseismic investigations, and seismic reflection methods. The northern Cascadia forearc is taking up most of the strain transmitted northward via the Oregon Coast block from the northward-migrating Sierra Nevada block. The north-south contractional strain in the Cascadia forearc is manifest in Holocene-active upper-plate faults in the Cascadia forearc, the northern-most components of which are the active faults at the northern margin of the Bellingham Basin.

1. INTRODUCTION

Forearcs are a critical component of many subduction zone plate boundaries for reasons both scientific and societal; from a tectonic standpoint, a substantial amount of plate boundary deformation can be accommodated in the forearc (North Island, New Zealand is an especially good example: Schermer et al., 2004; Kelsey et al., 1998; 1985), and from a societal standpoint, emergent forearcs house many of Earth's large population centers (pertinent to this discussion is the Puget lowland urban corridor in northwest Washington, USA). These population centers are at increased risk, not only from the seismic hazard associated with plate boundary earthquakes at convergent margins but also from the upper-plate earthquakes hosted in the forearc. Therefore, a more thorough understanding of the deformational setting of the northern Cascadia forearc, which sits above the convergent boundary between the subducting Pacific Plate and the overriding North American Plate at the latitude of Seattle, Washington, has societal as well as scientific value.

Despite a conceptual model for northern Cascadia forearc deformation, which is well grounded in GPS geodetic measurements and paleoseismic investigations of active faults, the tectonic structures that must necessarily accommodate forearc strain are incompletely understood at the northern end of the northern Cascadia forearc. In particular, the hypothesis of a migrating forearc implies that the northern, leading edge of the deforming forearc may be a dynamic boundary zone that incorporates new active deformation.

What is northern end of the actively deforming northern Cascadia forearc and where are the active faults that comprise this northern boundary? Wells et al. (1998) proposed that the northern Cascadia forearc impinged northward against stable North America at roughly the latitude of the east-trending Devils Mountain fault zone (Figure 1B). The model of Wells et al. (1998) focused on fault structures in the southern Puget lowland with a backstop in northern Puget Sound. Subsequent tectonic

summaries (Johnson et al., 2004b) also adopted this model. But recent investigations (Barnett et al., 2006) show that active faults, which accommodate north-south shortening, occur 50-60 km north of the predicted backstop of the Devils Mountain fault zone and only 8 km south of the international border.

The objective of this paper is to lay out a revised tectonic framework for the migrating forearc that identifies a tectonically active basin (Bellingham Basin) at the northern end of the deforming forearc. The paper defines the faults within, and on the margins of, this basin; these faults comprise the northern, leading edge of the deforming northern Cascadia forearc.

2. GEOLOGIC SETTING

The margin-parallel northward migration of the Oregon Coast block (McCaffrey et al., 2000) causes shortening of the Cascadia forearc basin region north of the leading edge of the block (Wells et al., 1998) (Fig. 1). GPS geodetic measurements confirm that the Cascadia forearc is moving north to northwestward (Mazzotti et al., 2003). The Cascadia forearc abuts against a backstop to the north with no margin-parallel motion, and the forearc is shortening at a rate of approximately 4.5 mm/yr (Mazzotti et al., 2002). This margin-parallel shortening is concentrated in the region of high crustal seismicity along the Puget lowland corridor between Olympia and the US/Canadian border (Mazzotti et al., 2002).

Several east-west or southeast-northwest trending, Holocene-active fault zones in the Puget lowland collectively accommodate north-south forearc shortening in the upper plate of the Cascadia subduction zone. The fault zones include, from south to north, the Olympia fault zone (Sherrod, 2001), the Tacoma fault zone (Sherrod et al., 2004), the Seattle fault zone (Bucknam et al., 1992; Sherrod et al., 2000; Blakely et al., 2002; Nelson et al., 2003; Brocher et al., 2004; Kelsey et al., 2008), the Southern Whidbey Island fault zone, (Johnson et al., 1996; Kelsey et al., 2004; Sherrod et al., 2005), the Utsalady Point fault zone (Johnson et al., 2004a), the Devils Mountain fault zone (Johnson et al., 1999) and the Kendall trace of the Boulder Creek fault (Haugerud et al., 2005; Barnett et al., 2006) (Figure 1B). The Kendall trace of the Boulder Creek fault is a newly identified fault at the northern end the contracting forearc. Identification of such active faults at the northern end will result in a more complete inventory of structures that accommodate shortening in the forearc.

3. RESEARCH APPROACH

We employ residual gravity data to define the Bellingham Basin, which is the northern-most forearc basin. We then introduce aeromagnetic data, using gravity data to help constrain the magnetic data. Using this potential data, in conjunction with LiDAR imagery, we investigate potential candidates for active faults and folds within the northern-most forearc basin. We describe paleoseismic investigations of active faults and assess abrupt changes in relative sea level at coastal sites. Where possible, ground- and boat-magnetic surveys follow up at the locations of candidate active faults. Offshore seismic surveys aid in identifying active faults and correlating active faults onshore with active faults offshore. In summary, multiple investigative techniques enable us to define the Bellingham forearc basin, characterize the active deformation and provide a context for interpreting the deformation at the northern end of the Cascadia forearc.

4. BELLINGHAM BASIN – GEOPHYSICAL AND STRUCTURAL CONSIDERATIONS

4.1 The Bellingham structural basin

A north-trending alignment of negative gravity anomalies in western Oregon, Washington, and British Columbia reflects structural basins of the Cascadia forearc. These basins, extending from the Willamette Valley in Oregon to the Strait of Georgia in British Columbia, have diverse and complex tectonic origins, all ultimately caused by subduction of the Juan de Fuca plate beneath North America. Four basins in the Puget Lowland are particularly well displayed in gravity anomalies: the Tacoma, Seattle, Everett, and Bellingham basins (Figure 2). The southern three of these basins (Tacoma,

Seattle, and Everett) are structurally tied to fundamental crustal faults that cross the Puget Lowland and are known to have produced M_w 6.5-7.5 earthquakes in the last 15 ka. The Seattle fault, which produced a M_w 7 earthquake about 1100 years ago (Bucknam et al., 1992), is an east-striking, north-verging thrust fault that, over the course of the last 40 million years, has lifted its hanging wall (the Seattle uplift) up and over regions to the north, producing the Seattle basin now filled with up to 10 km of Oligocene and younger sedimentary rocks (e.g., Johnson et al., 1994; Pratt et al., 1997; Brocher et al., 2001). The active Tacoma fault lies along the southern margin of the Seattle uplift and forms the structural contact with the Tacoma basin to the south (Johnson et al., 2004b; Pratt et al., 1997). The Everett basin is bounded on its north margin by the Devils Mt. fault (Johnson et al., 2001) and on the southwest by the southern Whidbey Island fault (Johnson et al., 1996; Kelsey et al., 2004; Sherrod et al., 2008). These large faults and intervening basins apparently evolved due to compressive forces established by the northward migration and clockwise rotation of the Washington forearc against stable regions to the north, a process that has continued at approximately steady rates for the last 10 to 15 Ma (e.g., Wells et al., 1998; McCaffrey et al., 2007).

It is generally believed that the Devils Mt. fault (Figures 1 and 2) serves as the buttress between the northward migrating forearc and stable North America (e.g., Johnson et al., 2001). This hypothesis is inconsistent with the position of the Bellingham basin, however, which lies well north of the Devils Mt. fault. The location of the Bellingham basin suggests either that the buttress lies somewhere north of the Bellingham basin or that the Bellingham basin itself evolved independent of processes that formed the other Puget Lowland basins. Recent paleoseismic studies of the Boulder Creek fault (Figures 1 and 2; Barnett et al., 2006; Sherrod et al., in preparation) favor the former explanation: The Boulder Creek fault, which lies near the Canadian border, north of the Bellingham basin (or at the northern margin of the Bellingham Basin), and well north of the Devils Mt. fault, has produced earthquakes in Holocene time and is apparently contributing to northward shortening of the forearc.

4.2 Concealed crustal structure interpreted from magnetic anomalies

The northern margin of the Bellingham basin, as defined by its gravity anomaly, passes through Birch Bay-Drayton Harbor coastal zone, where our paleoseismic studies, described below, find evidence for tectonic deformation in late-Holocene time. No faults or folds are mapped in the immediate area of Birch Bay, and such structures, if they exist, could be concealed by Pleistocene and younger glacial deposits that completely cover the Birch Bay area (Easterbrook, 1963; 1976). Elsewhere in the Puget Lowland, analysis of high-resolution aeromagnetic data have proven useful in mapping and characterizing active faults, where, in concert with LiDAR topographic surveys and follow-on trench excavations, a rich history of Holocene deformation is now being revealed (e.g., Sherrod et al., 2008; Blakely et al., 2002; 2009). Here we investigate aeromagnetic data from the Bellingham area to explore for and map concealed faults that may be responsible for late-Holocene deformation in the Birch Bay area. We focus on the coastal area between Bellingham Bay and Drayton Harbor (Figure 1C), which we will refer to as the Birch Bay study area after an embayment in this coastal reach.

Magnetic data from the Birch Bay area (Figure 3) were acquired in 1997 as part of an airborne magnetic survey of the entire Puget Lowland (Blakely et al., 1999). Measurements were made at a nominal elevation of 250 m above terrain along north-south lines spaced 400 m apart. Measurement altitudes ranged between 230 and 260 m throughout the northwest quarter of the study area, but were significantly higher over mountainous regions to the east. Total field measurements were converted to anomaly values by subtraction of the International Geomagnetic Reference Field, updated to the date of the survey. The anomalies in Figure 3 are transformed to the north magnetic pole in order to eliminate anomaly skewness and horizontal displacement caused by non-vertical directions of magnetization and ambient field (Blakely, 1995).

4.2.1 Magnetic lithologies in the Birch Bay area.

The magnetic field of the Birch Bay study area (Figure 3) is characterized by numerous high-amplitude magnetic anomalies, most of which are not obviously associated with mapped geology. A broad anomaly extends southwestward from north of the Vedder Mt. fault to the Georgia Strait (Figure 3, label A), an area entirely covered by Pleistocene and younger glacial outwash and other young sedimentary deposits. Glacial deposits in the Birch Bay area are weakly magnetic, with magnetic susceptibilities on the order of 0.003 SIU¹ (Tables 1 and 2), consistent with measurements of glacial deposits elsewhere in the Puget Lowland (Sherrod et al., 2008). While glacial deposits do produce low-amplitude anomalies in the Birch Bay area, they are insufficiently magnetic to produce the broad aspects of anomaly A. Thus, the lithologic source of anomaly A must lie concealed beneath the glacial deposits and within pre-Pleistocene basement.

Most basement rocks exposed elsewhere in the study area are insufficiently magnetic to cause anomaly A. Tertiary exposures are mainly continental sedimentary rocks of the Chuckanut Formation (e.g., Johnson, 1982), with magnetic susceptibilities typically <0.001 SIU (Tables 1 and 2). Moreover, most pre-Tertiary rocks, where exposed in the area, are not obviously associated with large magnetic anomalies. There is one important exception, however: Several high-amplitude anomalies of the study area overlie pre-Tertiary ultramafic rocks, notably anomalies over exposures north of the Boulder Creek fault (Figure 3a, label B) and in parts of the San Juan Islands (Figure 3, label C). Ultramafic rocks can be strongly magnetic, especially when they contain serpentinite (Tables 1 and 2). By inference, concealed pre-Tertiary ultramafic rocks may be responsible for anomaly A and for other high-amplitude anomalies in the area, including anomalies over the northern part of Lummi Island (Figure 3a, label D), immediately north of Whatcom Lake (Figure 3, label E), and northwest of the Twin Sisters Range (Figure 3, label F).

We also should consider the possibility that anomaly A and other anomalies in the study area are caused by lithologies entirely unexposed in the study area. Well logs in the Bellingham area, for example, describe 100 to 200 m of Quaternary deposits overlying Miocene and older continental sediments that include a pebble conglomerate (Hopkins, 1968). This Miocene conglomerate is not exposed anywhere in the study area as far as we know, but well logs describe it as being similar to the Miocene Blakely Harbor Formation exposed elsewhere in the Puget Lowland (Fulmer, 1975). The Blakely Harbor Formation is significantly magnetic where it crops out on Bainbridge Island, and it produces pronounced linear magnetic anomalies where deformed by the Seattle fault (Blakely et al., 2002). It is possible that the concealed Miocene conglomerate encountered in wells is the cause of anomaly A.

4.2.2 Magnetic lineaments and paleoseismic deformation

A complex pattern of short-wavelength, low-amplitude magnetic anomalies is superimposed on anomaly A (Figure 4) and may have implications for late-Holocene deformation observed at our paleoseismic sites. The short wavelengths of these anomalies indicate that they originate from near the topographic surface, within or just below Pleistocene glacial cover and above the source of the broader aspects of anomaly A itself. The procedure that illuminates the short-wavelength pattern (Figure 4) has two steps: original measurements were analytically continued to a surface 50 m higher than the elevation of the measurements and then subtracted from the original data. This procedure is equivalent to a discrete vertical derivative, a method that amplifies shallow-source anomalies at the expense of anomalies of deeper origin (Blakely, 1995). Thus, anomaly A in Figure 4 has been subdued relative to lineaments originating from sources nearer the topographic surface.

A large number of magnetic lineaments are evident in the filtered magnetic data (Figure 4), especially in the region east of Birch Bay and Drayton Harbor. Lineaments are typically less than 5 km in length, but in some cases extend for distances >10 km. The magnetic lineaments in Figure 4 are

¹ Susceptibility is a dimensionless quantity, with a value that depends on the system of units. SIU is an abbreviation for *le Système international d'unités*, or International System of Units.

similar in character to anomalies observed along the mainland portion of the southern Whidbey Island fault south of Everett (Sherrod et al., 2008), where the lineaments are associated with LiDAR topographic scarps and are caused by offsets in late Pleistocene and younger glacial deposits. We here consider the possibility that some of the lineaments in the Birch Bay study area are similarly caused by shallow crustal faults. To assist with our interpretation, we applied a method that numerically and objectively calculates the position of contrasting magnetization from the shape of magnetic anomalies (Figure 4, black dots; Blakely, 1995; Phillips et al., 2007).

A regional interpretation of the gravity and magnetic anomalies (Figure 5), based on Figures 2, 3 and 4, shows linear zones of inferred uplift bounded on one or both sides by interpreted magnetic contacts, which are indicated by red dotted lines. Several northwest-striking magnetic contacts are evident crossing from offshore to onshore regions in the vicinity of Drayton Harbor, Birch Bay, and Lummi Bay. Each of these is spatially associated with sites of late-Holocene deformation, as discussed below, suggesting that the lineaments could be caused by concealed, active faults.

Drayton Harbor magnetic lineament. The northwest-striking lineament through Drayton Harbor (Figure 5, label DH) is roughly parallel to a topographic alignment observed in LiDAR data (Figure 5, blue lines). The LiDAR image of the Drayton Harbor topographic scarp is discussed in the next section. The topographic alignment includes both north-side-up and south-side-up scarps on late Pleistocene surfaces. North-side-up scarps occur along the north side of a small stream valley and probably reflect fluvial processes. South-side-up scarps, however, do not appear to be fluvial in nature and may be caused by tectonic processes (see below). The sense of the magnetic anomaly across the Drayton Harbor, with higher magnetic values south of the lineament, is consistent with south-side-up displacement of weakly magnetic, normally magnetized strata. The magnetic lineament and topographic alignment are roughly parallel to each other, but their mapped positions are not precisely equivalent. Differences in their mapped details are expected, considering that the magnetic anomaly originates from depth. The topographic scarps seen in LiDAR data may be splays extending to the surface from a concealed through-going fault at depth manifested in the magnetic data.

The Drayton Harbor magnetic lineament, as mapped on Figure 5, extends ~25 km from the Strait of Georgia to onshore regions (Figure 5, label DH). The lineament has northwest strike through Drayton Harbor but rotates to an east-west trend farther east. At its eastern end, the Drayton Harbor lineament appears to merge with a discontinuous series of positive anomalies that extend northeastward to beyond the town of Sumas (Figure 5, label SF).

Birch Bay magnetic lineament. A second northwest-striking magnetic lineament passes through Birch Bay (Figure 5, label BB) and makes landfall at our Birch Bay and Terrell Creek paleoseismic site (see below). North of the magnetic lineament, beach terraces are elevated ~5 m relative to modern shorelines, whereas elevated beach terraces are not present south of the magnetic lineament. The sense of the magnetic anomaly, with higher anomaly values north of the lineament, is consistent with a north-side-up fault located precisely at the beach-terrace inflection point. We suggest that the Birch Bay magnetic lineament (Figure 5, label BB) reflects a concealed north-side-up fault, at least 23 km long, responsible for late-Holocene earthquakes and for the 5-m uplift of beach terraces immediately to its north.

Sandy Point magnetic lineament. A third northwest-striking magnetic lineament extends from the Strait of Georgia, passes through Lummi Bay, and makes landfall at Sandy Point (Figure 5, label SP). Similar to the Birch Bay magnetic lineament, the sense of the magnetic anomaly, with higher anomaly values north of the lineament, is consistent with a north-side-up fault located to the south offshore of Sandy Point. Therefore the zone of inferred uplift would include the Sandy Point coastal plain. A series of uplifted late Holocene beach ridges are exposed on this coastal plain (see further discussion below), and the inferred north-side-up fault is not inconsistent with coseismically uplifted beach berms on the Sandy Point coastal plain.

5. PALEOSEISMIC INVESTIGATIONS

5.1 Approach: LiDAR investigations and relative sea level investigations at sites affected by active Tectonics

We utilized high resolution digital elevation models, derived from LiDAR data sets, to evaluate whether the land surface shows evidence of displacement by Holocene faulting or folding, especially along magnetic lineaments delineated in Figure 5. Two LiDAR data sets were utilized. The first is an early 2005 leaf-off survey of the Lummi reservation acquired by the Puget Sound LiDAR Consortium (<http://pugetsoundlidar.ess.washington.edu>) on behalf of the Lummi Nation (Figure 6). The design pulse density was $>1/\text{sq meter}$. The second is a summer 2006 leaf-on survey over the remainder of western Whatcom County and western Skagit County acquired by the U.S. Geological Survey in cooperation with Washington Department of Natural Resources, Skagit County, and Whatcom County. The second survey had a pulse density of $>0.5/\text{sq meter}$.

Late Pleistocene and Holocene landforms are clearly visible on LiDAR images filtered to depict only bare-earth returns. Landforms associated with ice-margin processes, late Quaternary glacial runoff channels and glacial-isostatic-induced sea level changes (Kovanen and Easterbrook, 2002; Kovanen and Slaymaker, 2003) are common on the images. Superimposed on these ice-loading-related and glacial-process-generated landforms are three landforms, visible on the LiDAR, that implicate Holocene tectonic processes. These landforms include a linear topographic scarp that we infer is a candidate fault scarp (Drayton Harbor scarp), late Holocene uplifted beach storm berms (evident at Sandy Point) and uplifted late Holocene bay or estuarine flats (evident at Tennant Lake and Birch Bay). The Lummi Nation LiDAR survey proved exceptionally useful for identifying late Holocene uplifted coastal landforms at Sandy Point. To further investigate the LiDAR-identified candidate fault scarp, ground-magnetic transects were completed across the Drayton Harbor LiDAR scarp.

Relative sea level studies from multiple coastal sites collectively provide information on the timing and style of coastal deformation caused by late Holocene earthquakes. Tectonically stable sites in the Puget lowland have submerged in the last few thousand years (Beale, 1990). If there is no tectonically-induced differential vertical crustal displacement along the northwestern Washington coast, then the relative signal at all coastal localities should be the same and should record gradual submergence. We investigated the history of relative sea level at six sites where landforms and Holocene deposits collectively provide information on relative sea level change in the late Holocene; from south to north these sites are Chuckanut Cove, Sandy Point, Tennant Lake, Terrell Creek and Drayton Harbor (Figure 6).

5.2. Drayton Harbor fault scarp

The Drayton Harbor scarp, as mapped on LiDAR, is an up-to-the-south scarp that extends a minimum of 7 km from the town of Blaine and the northeastern part of the Drayton Harbor embayment east-southeastward subparallel to Dakota Creek. The scarp is expressed both by topography and by disrupted drainage (Figure 7).

We infer the scarp is a fault and not an erosional feature. The scarp is not the eroded edge of a channel because first, the up-to-the south scarp is subparallel to up-to-the-north terrace risers on the northern side of the Dakota Creek valley; second, the scarp cuts across different terrace levels; and third, the scarp is not confined to one fluvial surface.

5.2.1. Ground Magnetic Survey of Drayton Harbor Scarp

To further assess whether the LiDAR scarp could be a fault scarp, we were able to acquire several key ground-magnetic transects across the Drayton Harbor LiDAR scarp (Figures 5 and 8, label DH). Transects were conducted on foot using a cesium-vapor magnetometer integrated with GPS and carried in a backpack frame. Measurements were made at 1-second intervals while walking at normal speeds. A stationary proton-precession magnetometer was operated continuously to measure and

correct for time-varying fields. All transects are shown in Figures 8, where they have been low-pass filtered at a 200-sec cutoff.

Magnetic profiles across the Drayton Harbor LiDAR scarp (Figure 8) closely mimic filtered aeromagnetic anomalies (Figure 4) and more precisely define the location of the magnetic contact. Each transect exhibits a sharp magnetic gradient, positive to the south and closely aligned with the magnetic contact numerically determined from the aeromagnetic data. Along Valley View Drive, for example, the magnetic field rises 135 nT from north to south over a distance of 540 m. The steepest gradient along Valley View Drive falls approximately 100 m south of the magnetic contact determined from aeromagnetic data and about 130 m north of the actual lidar scarp.

Ground-magnetic and aeromagnetic data support the inference that the Drayton Harbor scarp is the surface expression of a fault rather than being caused by surface erosional processes. We suggest that the ground-magnetic and aeromagnetic anomalies manifest concealed stratigraphy in the upper crust deformed by the same tectonic structure that is responsible for the topographic scarp. The magnetic lineament may reflect a fault that juxtaposes magnetic lithologies to the south, possibly pre-Tertiary rocks, against weakly magnetic Quaternary deposits to the north. Based on the amplitude and width of the steepest gradient along Valley View Drive, the top of the contact is located several hundred meters below the earth's surface. Although the magnetic and topographic lineaments are generally parallel, they are clearly not coincident. The magnetic gradient, in particular, is significantly more sinuous than the scarp. We view these differences as reflecting complexities of the concealed deformation and its association with surface faulting.

5.3. Abrupt Subsidence at Terrell Creek Marsh

The Terrell Creek marsh is situated landward of a shore berm within the estuarine reaches of lower Terrell Creek (TC, Figure 6; Figure 9). The creek is bounded by a low terrace ('upland' in Figure 9 inset) and the surface of the marsh consists of freshwater peat. Mud at ~1.4 m depth below the surface contains estuarine shells. A buried freshwater peat underlies Terrell Creek marsh at 70 cm depth. Deposited on the upper contact of the freshwater peat is a 1 mm-thick fine-to-very-fine, well sorted sand (Core TC06B, Figure 6; see location of this core on Figure 9). This former freshwater marsh is overlain by about 25 cm of tidal mud and then overlain by the freshwater peat that makes up the modern marsh surface.

Timing and nature of the environmental change that occasioned burial of the freshwater marsh indicates the change was recent and sudden. Diatom biostratigraphic data in core TC06B (Figure 10), obtained by sampling across the upper contact of the buried peat, indicates that the marsh changed environmental conditions abruptly from a peaty freshwater wetland to a tidal mudflat. The radiocarbon-based age of the peaty freshwater wetland underneath the tidal flat, derived from detrital twigs in the peat, is 1390-1290 yrs B. P. (Table 3, youngest of two detrital-wood ages). Therefore, the abrupt environmental change to tidal flat occurred shortly after 1400 years ago.

On the basis of our work at Terrell Creek marsh, we infer that Terrell Creek estuary abruptly subsided in the late Holocene, and then gradually reemerged to be the freshwater marsh of today. From our coring program that consisted of 21 cores in three transects over the length and width of the marsh (Figure 9), we infer that the subsidence event affected the entire marsh and local estuarine area and that the abrupt subsidence was a tectonic response to an earthquake. We infer that the environmental change records an episode of abrupt submergence that allowed tidal inundation of the freshwater marsh and deposition of tidal sediment. The marsh then re-emerged to host a peaty freshwater wetland again.

At the contact between the abruptly subsided freshwater peat and the overlying tide flat mud is the 1 mm-thick, fine-to-very-fine, well sorted sand. This sand deposit, although thin, was present at the same contact position in most of the 21 cores that we described across the Terrell Creek estuary. We infer that the sand was transported to the Terrell Creek estuary by a tsunami triggered by the ca. 1400 yr B.P. earthquake that caused coseismic subsidence of the Terrell Creek marsh.

5.4. Emerged Estuary at Birch Bay: Abrupt vertical crustal displacement in the Late Holocene

At Birch Bay (site BB, Figure 6; Figure 9) at least one abrupt uplift event has occurred in the late Holocene, raising a tide flat above modern high tide levels. The town of Birch Bay sits on a beach berm on the shores of Birch Bay (Figure 1); and the flat, elevated coastal plain inland of the berm is only a few meters above high tide level. We investigated the Birch Bay coastal plain with a suite of 12 cores (Figure 9) and follow-up radiocarbon dating and biostratigraphic investigation.

5.4.1. Stratigraphy at Birch Bay

The stratigraphy beneath the Birch Bay coastal lowland is invariant and consists, in general, of two units (core BB06B, Figure 6). The lower unit is greenish gray, soft, estuarine mud and is abruptly overlain by the upper unit, which is a freshwater peat. The contact between these two units occurs at a shallow depth that ranges from 25 cm at inland sites to 45 cm near the coast. At this major contact, the stratigraphy has important additional complexity. In some cores, the estuarine mud changes color in the upper few centimeters just below the peat. In other cores, there appears to be a few cm-thick increase in mud sedimentation within the peat above the major contact. Because of these subtle stratigraphic features may indicate subtle shifts in environment after or before the major shift from tidal to freshwater peat, we undertook detailed diatom biostratigraphic investigation in the decimeters that bracket the mud-to-peat transition in core BB09-D (see core location on Figure 9)

5.4.2. Biostratigraphy at Birch bay

From the vertical distribution of diatom flora within the core BB09-D (Figure 10), there are two transitions that separate three biostratigraphic units. Three diatom zones define the three biostratigraphic units (Figure 10).

Diatom zone 1 is in the lower part of the core (Figure 10) and is dominated by marine diatoms - mostly *Scolecioneis tumida*, *Gyrosigma balticum*, *Grammatophora oceanica*, and *Paralia sulcata*.

Diatom zone 1, with the upper limit at 44 cm depth, corresponds to the gray marine mud (Figure 10).

Diatom zone 2 is between 44 and 33 cm depth and consists of both marine and brackish diatoms (Figure 10). This zone is dominated by several diatoms - *Diploneis interrupta* (marine/brackish), *Paralia sulcata* (marine), *Aulacoseira italica* (low salinity brackish to freshwater), *Tabellaria fenestrata* (freshwater), *Pinnularia viridis* (freshwater), and *Eunotia prarupta* (freshwater). The dominant diatoms, representing a mixture of marine, marine/brackish and freshwater affinities, together define a brackish marsh environment, which is ideal for brackish marsh diatom floras.

Diatom zone 3 is in the upper third of the core and is dominated by freshwater diatoms (Figure 10). The diatom zone floras were poorly preserved, but the floras are typical of shallow-water freshwater marsh environments similar to freshwater marsh diatom floras observed on the Birch Bay coastal plan today.

The most striking transition is from zones 1 to 2. Most of the brackish marsh flora appears very abruptly at 44 cm in depth (the mud-peat contact), and several brackish aerophiles (soil diatoms) appear only in this part of the core. There are two viable options to cause this transition. It could occur if the area had a high sedimentation rate and finally shoaled enough to let marsh vegetation take hold. Our preferred alternative, preferred because it is supported by the local coastal geomorphology, is that tectonic uplift caused the transition.

Reconstruction of environment from diatoms (Birks, 1995; Hemphill-Haley, 1995; Juggins, 1998) provide estimates of amount of relative sea level fall and therefore amount of tectonic uplift.

The site appears to start going up at about 52 cm in depth and does not get to near present elevation environmentally, until around 35 cm in depth (Figure 10). Uplift may have been gradual at first and then abrupt. Taking error into account in the environmental reconstruction from diatom flora, the site clearly went up tectonically between 52 cm and 35 cm by at least 50 cm, but tectonic uplift could have been as much as 2 m.

The abrupt transition from marine to freshwater environments observed in the Birch Bay stratigraphy therefore requires an uplift of as much as 2 m, and therefore we infer that the flat elevated

coastal plain inland of the berm is a raised estuary that was coseismically uplifted and abandoned. Between the raised estuary and the modern berm-and-mud-flat of Birch Bay, there is a raised berm that probably was the beach berm at the time the raised estuary was a tide flat.

We infer the lower Terrell Creek valley bottom abruptly subsided at about the same time in the late Holocene that Birch Bay townsite abruptly uplifted to a freshwater environment. A buried fault between the two sites (Figure 9) could accommodate the synchronous uplift and subsidence at the two adjacent sites. The fault must be buried because there is no fault scarp at the location where the fault must intersect the ground surface in order to accommodate uplift to the north and subsidence to the south.

5.4.3. Detailed marine magnetic survey of Birch Bay and surrounding areas

A prominent northwest-striking magnetic anomaly is apparent in airborne magnetic data (Figure 4 and 5, label BB) crossing Birch Bay and extending onshore for several kilometers. The anomaly occurs at the inferred trace of the Holocene fault separating uplifted coastal plain at Birch Bay from subsided marsh at Terrell Creek (Figure 9). The southwestern margin of the Birch Bay magnetic anomaly coincides closely with the southern limit of an uplifted beach terrace at Birch Bay, and thus the anomaly may reflect uplifted, slightly magnetic stratigraphy in the subsurface. If so, the magnetic anomaly allows us to map the location of the uplift both northwest and southeast of the beach terrace. To understand the Birch Bay magnetic anomaly in greater detail, we conducted a detailed magnetic survey of Birch Bay and surrounding marine areas (Figure 11).

The marine-magnetic survey was conducted with a 5-m-long fishing boat, powered by a single outboard motor and navigated with GPS. The boat was constructed of fiberglass and aluminum and thus was essentially nonmagnetic. The motor did produce a small magnetic field, however, which was minimized by positioning the magnetic sensor, a cesium-vapor magnetometer, at the end of a 3.4-m-long wooden pole extending forward from the bow of the boat. Overall, the magnetic field of the boat and motor produced a maximum heading error of 13 nT, which was removed from the data using standard algorithms. A proton-precession magnetometer was stationed at a fixed location nearby and operated during the entire survey in order to measure and subsequently remove diurnal and transient magnetic fields. Total-field anomalies were computed by subtracting the International Geomagnetic Reference Field on the days of the survey. The marine survey was conducted along northeast-directed track lines spaced 500 m apart (Figure 11); four northwest-directed tie lines were included to check for cross-track consistency. After heading corrections were made, the 56 crossings of tie lines and track lines had an average absolute crossing error of 0.06 nT, approximately 0.6 percent of the total field at each crossing.

It is evident from Figures 4 and 11 that magnetic anomalies seen in aeromagnetic data, when filtered in order to emphasize shallow magnetic sources, are also present in ocean-surface measurements. While this is not a surprising observation, it clearly demonstrates that our filtering methodology applied to aeromagnetic data is useful in illuminating near-surface lithologies and tectonic structures. The magnetic field in marine areas surrounding Birch Bay is dominated by northwest-striking anomalies, possibly reflecting folded and faulted lithologies in the near surface. The Sandy Point magnetic anomaly (Figures 5 and 11, label SP) extends across the entire marine survey, and the Birch Bay anomaly (Figures 5 and 11, label BB) extends entirely across Birch Bay.

The southwestern margin of the Birch Bay magnetic anomaly coincides with the southern margin of the uplifted beach terrace, suggesting that the anomaly is caused by slightly magnetic stratigraphy raised closer to the earth's surface by the uplift. To further illuminate this contact, we also conducted a ground-magnetic transect around the Birch Bay shoreline (Figure 11). The transect was walked during low tide and as far west as possible in order to minimize cultural noise from the local community. A pronounced 50-nT positive anomaly was observed on the transect (Figure 11), consistent with the airborne and marine magnetic data. The sharp gradient at the southern margin of the anomaly is located precisely at the southern margin of the uplifted beach terrace.

The Birch Bay magnetic anomaly does not appear to extend northwest beyond Birch Bay, suggesting either that the causative structure is confined to Birch Bay or that it loses its magnetic properties beyond Birch Bay. On the other hand, Figure 4 indicates that the Birch Bay magnetic anomaly does extend southeastward from the shoreline for several kilometers, where it is completely obscured by magnetic fields associated with a paper mill and aluminum smelter. The Birch Bay magnetic anomaly thus defined, from Birch Bay to the paper mill, is only about 5 km in length. However, we note that a linear, northwest-striking magnetic anomaly is located southeast of the paper mill and aluminum smelter and is on strike with the Birch Bay magnetic anomaly. This magnetic feature extends to a point about midway between Ferndale and Bellingham (Figures 4 and 5). We suggest that the northwest-striking lineament between Ferndale and Bellingham is the continuation of the Birch Bay magnetic anomaly. Viewed in this way, the Birch Bay magnetic anomaly extends from the northwestern edge of Birch Bay to north of Bellingham, a total distance of 24 km.

5.5. Abrupt uplift of the Tennant Lake beach-cut strath

The Tennant Lake marsh (site TL, Figure 6; Figure 12) consists of peat underlain by a strath surface at shallow depth (0.7-2.5 m). The strath surface is cut on late Pleistocene glaciomarine drift. A beach sand deposit, 2-5 cm thick, lies on top of the strath and the peat in turn overlies the sand (Figure 12).

The strath, formed on late Pleistocene glaciomarine drift, was cut in the late Holocene during relative sea level rise. Evidence that the strath was cut as sea level drowned the site during gradual relative sea level rise is the beach sand deposit and the freshwater peat that overlies the strath. Subsequent to submergence, the strath was elevated abruptly in the late Holocene, isolating the shoreline and strath backedge (“Uplifted Holocene shoreline”, Figure 12). We infer that the striated topography that occurs just south of (but not north of) the raised shoreline, which is clearly resolved on the LiDAR imagery (Figure 12), is part of a set of grooves eroded in drift by advance of Sumas stade ice (Kovanen and Easterbrook, 2002); and the ridges between the grooves were subsequently washed clean in the wave zone and exposed on a late Holocene shore platform that was then tectonically uplifted and preserved.

5.6. Three abrupt uplifts of the coastal plain at Sandy Point

Sandy Point (site SP, Figure 6; Figure 13) is at the southeast end of the Strait of Georgia and consists of a raised coastal plain with a sand spit developed at the south end (Figure 6). The east side of the Sandy Point coastal plain is banked against a Holocene-age paleo sea cliff cut in glaciomarine drift (Figure 13), and late Pleistocene shorelines are notched in the hillslopes above the paleo seacliff (Figure 13). The late Pleistocene shorelines were cut while relative sea level fell during glacio-isostatic rebound (Clague and James, 2002). The Sandy Point coastal plain has been uplifted three times in the late Holocene.

Multiple late Holocene shorelines on the sand spit at Sandy Point (yellow, green, purple: youngest to oldest; Figure 13) are preserved because of several instances of abrupt relative sea level fall. The oldest shoreline (depicted in purple, Figure 13B) is preserved near the eastern edge of the Holocene platform adjacent to the paleo sea cliff. The younger two shorelines are preserved at the south end of the Sandy Point coastal plain north of the northwest end of Bellingham Bay. The oldest of these two shorelines (depicted in green, Figure 13B) was abandoned by relative sea level fall shortly before a south-flowing coastal stream captured the headwaters of a larger stream that flowed westward across the uplands and across the Holocene platform to the Strait of Georgia. The relative sea level fall (that abandoned the shoreline) lowered the baselevel of the small south-flowing creek, causing headward erosion that captured and beheaded the creek flowing off the upland. As a consequence, the beheaded west-flowing drainage on the sand platform became abandoned (Figure 13B).

A north-trending transect across the south end of the Sandy Point coastal plain (transect X-Y, Figure 13C) shows three abandoned surfaces. Each surface is underlain by mud to sandy mud that appears to be of tidal flat origin. We excavated two soil pits across the middle terrace (SP-A and SP-B,

Figure 13C), and diatoms investigations reveal that this middle terrace is underlain by tide flat deposits (green unit at base of pit SP-A, Figure 6). Based on similar deposits underlying all three raised terraces, we infer that all three elevated terraces are underlain by tide flat deposits (Figure 13C).

We infer that the three abandoned tide flat surfaces document three coseismic uplift events that have occurred in the time since late Holocene sea level stabilized. From transect elevations, we can estimate the magnitude of coseismic uplift that occasioned the abandonment of each paleo tide flats. The coseismic uplift amounts are the differences between the elevations of the shoreline angles (the platform-sea cliff junction, depicted by the red squares in Figure 13C) for each adjacent terrace. Based on shoreline angle elevations, the younger two raised tide flats each appear to have been uplifted by a meter or less during two separate late Holocene earthquakes. A small branch from the youngest raised tide flat that had a radiocarbon age of 2320-2060 years B. P. (Table 3), from which we infer that the youngest coseismic uplift was after about 2,100 years ago. The oldest of the three raised tide flats, which comprises most of the Sandy Point terrace, appears to have been uplifted 2.0-2.5 m during the earliest recorded earthquake. The oldest raised tide flat has been cumulatively uplifted about 4 m (Figure 13C) by three late Holocene earthquakes.

5.7. Coastal sites with negligible or inconclusive late Holocene relative sea level change

The stratigraphy at Chuckanut Cove (site CC, Figure 6) is consistent with stratigraphic observations at tectonically stable sites. At Chuckanut Cove, stratigraphy as documented in cores consists of lithified glaciomarine drift overlain by a paleosol, in turn overlain by peat. The basal peat contact is at or below high tide level. We infer from these cores that the site records late Holocene submergence because glaciomarine drift and an overlying paleosol, which were formerly above sea level, are now submerged. Therefore Chuckanut Cove hosts gradual relative sea level rise in the late Holocene, a coastal response at sites without late Holocene tectonic uplift or subsidence.

The mudflat at Drayton Harbor (site DH, Figure 6) provides an inconclusive relative sea level trend. The mudflat is underlain at shallow depth (within a meter) by glaciomarine drift. The distinctive large boulders that litter the mudflat surface at low tide are winnowed from the glaciomarine drift as the drift is eroded by coastline retreat. Because the Drayton Harbor topographic scarp, < 1 km to the north of Drayton Harbor, is up to the south, one would expect there may be an emerged marine deposit or landform fringing Drayton Harbor. However, in the absence of a distinctive emergent landform on the inner (eastern) edge of Drayton Harbor, the late Holocene sea level trend at Drayton Harbor remains inconclusive.

6. SEISMIC REFLECTION DATA AND ACTIVE FAULTING

6.1. On-land seismic reflection data

To date, the one on-land seismic reflection data source we have recovered is an approximately 6 km-long, north-trending seismic reflection profile 1.3 km east of Birch Bay Washington (Hurst, 1991). The line shows poorly resolved faulting of late Tertiary strata at the approximate location of the inferred trace of the Holocene-active blind fault between Birch Bay and the mouth of Terrell creek. This on-land seismic reflection line was one of many shot by American Hunter Exploration, Limited, near Birch Bay (track lines on Figure 1C). So far, we have been unsuccessful in tracking down the original seismic data through private seismic data brokers.

6.2. Marine seismic reflection data

Our approach is to evaluate whether faults inferred from marine seismic reflection profiles occur along the same trends as linear, steep gradients on flanks of magnetic anomalies. The track lines for the marine seismic reflection surveys are depicted on Figure 1C. Pre-existing industry lines are supplemented by sparker profiles. The marine seismic lines show several instances of possible Holocene deformation on structures approximately 5-15 km offshore to the west. Initial inspection of these data

reveals that Holocene sediment is deformed on the flanks of bedrock cored bathymetric highs. One of the deformation zones trend southeast onshore to the approximate vicinity of Sandy Point.

6.3. Faulting imaged on Sparker profiles correlated to onshore deformation

Sparker profiles, attained in 2005 by T. Pratt and M. Holmes through the University of Washington School of Oceanography, show highly resolved images of Holocene deformation of sediment on the flanks of bedrock cored bathymetric highs. One sparker profile (denoted by “Profile” in Figure 1C) depicts Holocene sediment, within 40 m of the sea floor, warped within a fold that is growing on the flank of a bedrock ridge (Figure 14). The ridge likely is the uplifted block of an active blind fault. The location and northwest trend spatially coincides with an offshore, northwest trending shallow aeromagnetic anomaly (Figure 14), and the sense of offset of the uplifted flank of the bedrock ridge, up to the northeast, is also with the aeromagnetic anomaly. This aeromagnetic anomaly trends to the southeast onshore to a location just offshore to the south of Sandy Point (Figure 14). Therefore, the fault that caused the series of Holocene coseismic uplifts of the Sandy Point shoreline probably is the same fault that deforms Holocene sediment that is imaged the sparker profile (Figure 14).

7. DISCUSSION AND CONCLUSION

7.1. Active faults, their regional extents and relationship to Bellingham basin

In this study we identify three previously unrecognized active, upper-plate faults that have trace lengths that extend from offshore to onshore based on aeromagnetic data. The three faults have been active in the Holocene based on LiDAR and paleoseismic investigations. These three fault, from north to south, are the Drayton Harbor, Birch bay and Sandy Point faults (Figure 15).

The Drayton Harbor, Birch Bay and Sandy Point faults lie along, or near, the northern margin of the Bellingham basin, as defined by regional gravity anomalies (Figure 5). In fact, the steepest gravity gradient passes directly through Birch Bay. We believe the association of active faults with the northern basin margin is more than coincidence and suggest that the fault traces manifest shallow crustal faults responding to northward migration of the Cascadia forearc and the continuing evolution of the Bellingham basin.

7.2. Integrative Characterization of the Deforming Cascadia Forearc

The Bellingham Basin is the northern of four basins, defined by regional gravity anomalies, that define the northern Cascadia forearc (Figure 2). Multiple data sets provide evidence that active faults occur within, and on the margins of, the Bellingham basin and the three other forearc basins to the south. With the recognition of the northernmost faults that bound part of the northern edge of the Bellingham Basin, there is – to a first order - a complete framework inventory of basins and faults that comprise the deforming Cascadia forearc basin.

Most of the strain within the deforming Cascadia forearc is concentrated at the northern and southern margins of the four basins (Figure 2). In detail, however, the fault patterns are complex. Shortening on individual faults must be dissipated through strike slip on the forearc margin or continuation of contractional shortening to the east to the Cascade Mountains or to the west to the eastern foothills of the Olympic Mountains (e. g., Blakely et al., 2009).

The deforming Cascadia forearc may be taking up most of the strain transmitted north from northward migration of the Sierra Nevada block. The actively deforming forearc abuts against the Canadian Coast Range to the north and is pushed from the south by the Oregon Coast Range block (Figure 1A). The Oregon Coast Range block relays motion from the Sierra Nevada block, which records little internal deformation. The Oregon Coast block probably records some internal deformation but active faults are not nearly as numerous, nor slip rates as large, as the active faults in the deforming Cascadia forearc to the north. Therefore the Cascadia forearc is taking up most of the strain transmitted from the northward-migrating Sierra Nevada block, and this strain is manifest in

Holocene-active upper-plate faults that bound the margins of four structural basins within the northern Cascadia forearc.

REFERENCES

- Barnett, E A. Kelsey, H M, Sherrod, B L , Blakely, R J, Hughes, J F, Schermer, E R, Haugerud, R A Weaver, C S, and Siedlecki, E, 2006, Active faulting at the northeast Margin of the greater Puget Lowland: A paleoseismic and magnetic-anomaly study of the Kendall scarp, Whatcom County, Northwest Washington, *Eos Trans. AGU*, 87(52), Fall Meet. Suppl., Abstract S31A-0183.
- Beale, H., 1990, Relative rise in sea-level during the late Holocene at six salt marshes in the Puget basin, Washington, M. S. thesis, Western Washington University, Bellingham, 157 pp.
- Birks, H.J.B., 1995, Quantitative palaeoenvironmental reconstructions, in Maddy, D., Brew, J.S. (Eds.), *Statistical Modeling of Quaternary Science Data*, Quaternary Research Association, Cambridge, pp. 161-254.
- Blakely, R.J., 1995, *Potential Theory in Gravity and Magnetic Applications*, 441 p., Cambridge Univ. Press, New York.
- Blakely, R.J., Wells, R.E., and Weaver, C.S., 1999, Puget Sound aeromagnetic maps and data: U.S. Geological Survey Open-File Report 99-514, <http://geopubs.wr.usgs.gov/open-file/of99-514>.
- Blakely, R. J., Wells, R. E., Weaver, C. S. and Johnson, S. Y., 2002, Location, structure, and seismicity of the Seattle fault zone, Washington, Evidence from aeromagnetic anomalies, geologic mapping, and seismic-reflection data, *Bull. Geol. Soc. Am.*, 114, 169– 177, doi:10.1130/0016-7606(2002)114<0169:LSASOT>2.0.CO;2.
- Blakely, R.J., Sherrod, B. L., Hughes, J. F., Anderson, M. L., Wells, R. E. and C.S. Weaver, C. S., 2009, Saddle Mountain fault deformation zone, Olympic Peninsula, Washington: Western boundary of the Seattle uplift, *Geosphere*, 5, 105–125, doi: 10.1130/GES00196.1.
- Brocher, T. M., T. Parsons, R. J. Blakely, N. I. Christensen, M. A. Fisher, R. E. Wells, and SHIPS Working Group, 2001, Upper crustal structure in Puget Lowland, Washington: Results from 1998 Seismic Hazards Investigation in Puget Sound, *J. Geophys. Res.*, 106, 13,541–13,564, doi:10.1029/2001JB000154.
- Brocher, T.M., Pratt, T.L., Spence, G.D., Reidel, M. and Hyndman, R.D., 2003, Wide-angle seismic recordings from the 2002 Georgia Basin geohazards initiative, northwestern Washington and British Columbia, U. S. Geological Survey Open-File Report 03-160. (<http://geopubs.wr.usgs.gov/open-file/of03-160/>).
- Brocher, T.M., Blakely, R. J. and Wells, R.E., 2004, Reinterpretation of the Seattle uplift, Washington, as a passive roof duplex, *Bull. Seis. Soc. Am.*, 94, 1379–1401, doi: 10.1785/012003190.
- Bucknam, R. C., Hemphill-Haley, E., and Leopold, E. B., 1992, Abrupt uplift within the past 1700 years at southern Puget Sound, Washington, *Science*, 258, 161-1614, doi:10.1126/science.258.5088.1611.
- Clague, J. J. and James, T. S., 2002, History and isostatic effects of the last ice sheet in southern British Columbia, *Quaternary Science Reviews*, 21, 71-87.
- Dragovich , J.D., R.L. Logan, H.W. Schasse, T.J. Walsh, W.S. Lingley, Jr., D.K. Norman, W.J. Gerstel, T.J. Lapen, J. E. Schuster, and K.D. Meyers, 2002, Geologic map of Washington—northwest quadrant, Washington Div. of Geol. and Earth Res. Geol. Map GM-50, 72 p., 3 plates.
- Easterbrook, D.J., 1963, Late Pleistocene glacial events and relative sea level changes in the northern Puget lowland, *Geological Society of America Bulletin*, 74, 1465-1484.
- Easterbrook, D.J., 1976, Geologic map of western Whatcom county, Washington, U.S. Geological Survey, Miscellaneous Investigation Series, Map I-854-B, scale 1:62,500.

- Fulmer, C.V., 1975, Stratigraphy and paleontology of the type Blakeley and Blakely Harbor Formations: Annual Convention of the Society of Economic Paleontologists and Mineralogists, Paleogene Symposium and Selected Technical Papers, Long Beach, California, April 1975, p. 210–271.
- Haugerud, R.A., Sherrod, B.L., Wells, R.E., and Hyatt, T. 2005, Holocene displacement on the Boulder Creek fault near Bellingham, Washington and implications for kinematics of deformation of the Cascadia forearc, Abstracts with Programs, Geological Society of America, 37(7), p.476.
- Hemphill-Haley, E., 1995, Diatom evidence for earthquake-induced subsidence and tsunami 300 yr ago in coastal Washington, *Geol. Soc. Am. Bull.*, 107, 367-378.
- Hopkins, W. S., 1968, Subsurface Miocene rocks, British Columbia-Washington, a palynological investigation, *Geological Society of America Bulletin*, 79, 763-768.
- Hurst, P.D., 1991, Petroleum geology of the Bellingham basin, Washington, and evaluation of the AHEL and Partners Birch Bay No. 1 well, *Washington Geology*, 19, 16-18.
- Johnson, S. Y., Potter, C. J. and Armentrout, J. M., 1994, Origin and evolution of the Seattle Fault and Seattle Basin, Washington, *Geology*, 22, 71– 74, doi:10.1130/0091-7613(1994)022<0071:OAEOTS>2.3.CO;2.
- Johnson, S. Y., C. J. Potter, J. M. Armentrout, J. J. Miller, C. A. Finn, and C. S. Weaver, 1996, The southern Whidbey Island Fault: An active structure in the Puget Lowland, Washington, *Geol. Soc. Am. Bull.*, 108, 334– 354, doi:10.1130/0016-7606(1996)108<0334:TSWIFA>2.3.CO;2.
- Johnson, S. Y., Dadisman, S. V., Mosher, D. C., Blakely, R. J., Childs, J. R., and Rhea, S. B., 1999, Neotectonics of the Devils Mountain fault and northern Whidbey Island fault, eastern Strait of Juan de Fuca and northern Puget Lowland, Washington: *Seismological Research Letters*, v. 70, p. 220.
- Johnson, S.Y., S.V. Dadisman, D.C. Mosher, R.J. Blakely, and J.R. Childs, 2001, Active tectonics of the Devils Mountain fault and related structures, northern Puget Lowland and eastern Strait of Juan de Fuca Region, Pacific Northwest, U.S. Geological Survey Professional Paper 1643, 45 p., 2 plates.
- Johnson, S. Y., et al., 2004a, Evidence for late Holocene earthquakes on the Utsalady Point Fault, northern Puget Lowland, Washington, *Bull. Seismol. Soc. Am.*, 94(6), 2299– 2316, doi:10.1785/0120040050.
- Johnson, S.Y., R.J. Blakely, W.J. Stephenson, S.V. Dadisman, and M.A. Fisher, 2004b, Active shortening of the Cascadia forearc and implications for seismic hazards of the Puget Lowland: *Tectonics*, 23, TC1011, doi: 10.1029/2003TC001507.
- Juggins, S., 1998, CALIBRATE version 0.82: A C++ program for analysing and visualising species environment relationships and for predicting environmental values from species assemblages, user guide version 1.0., unpublished computer program, 23 pp.
- Kelsey, H.M., Sherrod, B.L., Johnson, S.Y. and Dadisman, S.V., 2004, Land-level changes from a late Holocene earthquake in the northern Puget lowland, Washington, *Geology*, 32, 469-472.
- Kelsey, H. M., Sherrod, B. L., Nelson, A. R., and Brocher, T. M., 2008 Earthquakes generated from bedding-plane-parallel reverse faults above an active wedge thrust, *Geological Society of America Bulletin*, 120, 1581-1597.
- Kelsey, H. M., A. Hull, S. Cashman, K. Berryman, P. Cashman, J. Trexler, and J. Begg, 1998, Paleoseismology of an active reverse fault in a forearc setting: the Poukawa fault zone, Hikurangi forearc, New Zealand: *Geological Society of America Bulletin*, 110, 1123-1148.
- Kelsey, H.M., Cashman, S.M., Berryman, K.R. and Beanland, S., 1995, Structural evolution along the inner forearc of the obliquely convergent Hikurangi margin, New Zealand; *Tectonics*, 14, 1-18.

- Kovnenen, D.J. and Easterbrook, D.J., 2002, Timing and extent of Allerod and Younger Dryas age (ca. 12,500-10,000 ¹⁴C yr BP) oscillations of the Cordilleran ice sheet in the Fraser Lowland, western North America, *Quaternary Research*, 57, 208-224.
- Kovnenen, D.J. and Slaymaker, O., 2003, Lake Terrell upland glacial resurgences and implications for late-glacial history, northwestern Washington state, U.S.A., *Can. J. Earth Sci.*, 40, 1767-1772.
- McCaffrey, R., Long, M. D., Goldfinger, C., Zwick, P. C., Nabelek, J. L., Johnson, C.K. and Smith, C., 2000, Rotation and plate locking at the southern Cascadia subduction zone, *Geophysical Research Letters*, 27, 3117-3120.
- McCaffrey, R., A.I. Qamar, R.W. King, R. Wells, G. Khazaradze, C. A. Williams, C.W. Stevens, J.J. Vollick, and P.C. Zwick, 2007, Fault locking, block rotation and crustal deformation in the Pacific Northwest, *Geophys. J. Int.*, 169(3), 1315-1340, doi:10.1111/j.1365-246X.2007/03371.x.
- Mazzotti, S. Dragert, H., Hyndman, R., Miller, M. M., and Henton, J., 2002, GPS deformation in a region of high crustal seismicity: N. Cascadia forearc, *Earth and Planetary Science Letters*, 198, 41-48.
- Mazzotti, S. Dragert, H., Henton, J., Schmidt, M., Hyndman, R., Jams, T., Lu, Y. and Craymer, M., 2003, Current tectonics of northern Cascadia from a decade of GPS measurements, *Journal of Geophysical Research*, 108, doi:10.1029/2003JB002653.
- Nelson, A.R., Johnson, S.Y., Kelsey, H.M., Wells, R.E., Sherrod, B.L., Pezzopane, S.K., Bradley, L., Koehler, R.D., and Bucknam, R.C., 2003, Late Holocene earthquakes on the Toe Jam Hill fault, Seattle fault zone, Bainbridge Island, Washington, *Geological Society of America Bulletin*, 115, 1388-1403.
- Phillips, J.D., R.O. Hansen, and R.J. Blakely, 2007, The use of curvature in potential-field interpretation: *Exploration Geophys.*, 38, 111–119, doi:10.1071/EG07014.
- Porter, S.C., and Swanson, T.W., 1998, Radiocarbon age constraints on rates of advance and retreat of the Puget lobe of the Cordilleran ice sheet during the last glaciation, *Quaternary Research*, 50, 205-213.
- Pratt, T. L., S. Johnson, C. Potter, W. Stephenson, and C. Finn, 1997, Seismic reflection images beneath Puget Sound, western Washington State: The Puget lowland thrust sheet hypothesis, *J. Geophys. Res.*, 102, 27,469– 27,489, doi:10.1029/97JB01830.
- Schermer, E.R., Van Dissen, R., Berryman, K.R., Kelsey, H.M. and Cashman, S.M., 2004, Active faults, paleoseismology, and historical fault rupture in northern Wairarapa, North Island, New Zealand, *New Zealand Journal of Geology and Geophysics*, v. 47, p. 101-122.
- Sherrod, B. L., 1999, Gradient analysis of diatom assemblages in a Puget Sound salt marsh—Can such assemblages be used for quantitative paleoecological reconstructions?, *Palaeogeography, Palaeoclimatology, Palaeoecology*, 149, 213–226.
- Sherrod, B.L., Bucknam, R.C., Leopold, E.B., 2000, Holocene relative sea-level changes along the Seattle Fault at Restoration Point, Washington, *Quat. Res*, 54, 384-393.
- Sherrod, B. L., 2001, Evidence for earthquake induced subsidence about 1100 yr ago in coastal marshes of southern Puget Sound, Washington, *Geological Society of America Bulletin*, 113, 1299-1311.
- Sherrod, B.L., Brocher, T.M., Weaver, C. S., Bucknam, R.C., Blakely R.J., Kelsey, H.M., Nelson, A.R. and Haugerud, R., 2004, Holocene fault scarps near Tacoma, Washington, USA, *Geology* 32, 9-12.
- Sherrod, B. L., Blakely, R.J., Weaver, C., Kelsey, H., Barnett, E. and Wells, R., 2005, Holocene fault scarps and shallow magnetic anomalies along the southern Whidbey island fault zone near Woodinville, Washington, U. S. Geological Survey, Open-File report 2005-1136, 35 p.
- Sherrod, B.L., R.J. Blakely, C.S. Weaver, H.M. Kelsey, E. Barnett, L. Liberty, K.L. Meagher, and K. Pape, 2008, Finding concealed active faults: extending the southern Whidbey Island fault

across the Puget Lowland, Washington, 2008, *J. Geophys. Res.*, 113(B05313), doi:10.1029/2007JB005060.

Simpson, R.W., R.C. Jachens, R.J. Blakely, and R.W. Saltus, R.W., 1986, A new isostatic residual gravity map of the conterminous United States with a discussion of the significance of isostatic residual anomalies: *J. Geophys. Res.*, 91, 8348–8372, doi: 10.1029/JB091iB08p08348.

Wells, R. E., C. S. Weaver, R. J. Blakely, 1998. Forearc migration in Cascadia and its neotectonic significance. *Geology* 26, 759-762.

Table 1. Magnetic susceptibility measurements from the Bellingham area. Measurements made on in situ rocks using a Kappameter model KT-5. Average values are geometric average of N samples. Average and standard deviation expressed in SI units times 1000

Site	Longitude	Latitude	N	Avg.	St. Dev.	Site Description
1	-122.10493	48.89286	10	0.66	0.36	Eocene Chuckanut Formation (sandstone)
2	-122.08320	48.89091	10	0.45	0.03	Eocene Chuckanut Formation (siltstone)
3	-122.05042	48.88617	10	0.26	0.03	Eocene Chuckanut Formation (sandstone)
4	-122.04807	48.89040	10	0.10	0.02	Eocene Chuckanut Formation (arkosic sandstone)
5	-122.04736	48.89472	10	0.26	0.05	Eocene Chuckanut Formation (various lithologies)
6	-122.11102	48.89598	10	2.45	0.64	Pleistocene glacial outwash
7	-122.19313	48.95596	10	0.37	0.16	Pre-Tertiary metamorphic rock, highly altered
8	-122.20062	48.93760	10	3.09	2.68	Pleistocene conglomerate (ultramafic pebbles)
9	-122.20247	48.93795	10	4.60	4.88	Pre-Tertiary ultramafic
10	-122.21074	48.93502	10	11.77	8.05	Pre-Tertiary ultramafic
11	-122.00025	49.00025	10	5.01	2.00	Pleistocene glacial outwash (sand, diamict)
12	-122.66890	48.97890	10	2.43	0.55	Pleistocene glacial outwash, glacial marine drift
13	-122.66025	48.98820	10	2.22	0.98	Pleistocene gravel (large pebbles in sand)
14	-122.63509	48.97134	10	3.84	1.20	Pleistocene outwash (clay, medium sand)
15	-122.79494	48.97592	10	3.99	0.56	Pleistocene glacial marine drift (silt, fine sand)
16	-122.77715	48.89853	10	2.65	0.54	Pleistocene glacial marine drift
17	-122.48196	48.66859	10	0.94	0.84	Eocene Chuckanut Formation (sandstone)
18	-122.48248	48.67151	10	0.86	0.83	Eocene Chuckanut Formation (sandstone)
19	-122.49046	48.65152	10	1.15	0.30	Eocene Chuckanut Formation (sandstone)
20	-122.48995	48.70067	10	0.15	0.04	Eocene Chuckanut Formation

Table 2. Summary of magnetic susceptibility measurements from the Bellingham area. Number of samples is the total number of measurements for each lithology. Confidence intervals are standard deviation divided by square root of the number of samples minus 1. Average, standard deviation, and confidence intervals expressed in SI units times 1000. See Table 1 for additional information.

Lithology	N Sites	N samples	Average	St. Dev	Conf. Int
Eocene Chuckanut Formation	9	90	0.54	0.38	0.06
Pleistocene glacial deposits	8	80	3.21	0.98	0.11
Pre-Tertiary ultramafic rocks	2	20	8.19	5.07	1.88

Table 3. Radiocarbon ages, coastal Whatcom County

Sample I.D.*	Laboratory I.D. **	Date ***	$\delta^{13}C$ ****	14C age *****	Calibrated 14C age range*****	Material
<u>Birch Bay:</u>						
BB 09 A 40X (40-41 cm)	B-274095	3.5.2010	-25.9	1700±40	1710-1530	Three 2-3 mm-long wood frags, one 5-mm long needle, one 2mm-diameter seed.
BB 09 D 37B (37-39 cm)	B-274096	3.5.2010	-28.2	2080±40	2150-1940	Bulk peat sample.
BB 09 D 41 (41-42 cm)	B-274097	3.5.2010	-27.4	1690±40	1700-1520	Twenty 0.5-2.0 mm-long wood fragments.
<u>Terrell Creek:</u>						
TC 06 B 66.5	B-240535	2.28.2008	-24.7	1430±40	1390-1290	One wood stem detrital fragment, 18 mm long.
TC 07 C50 76 (76-77 cm)	B-240537	2.28.2008	ND	1500±40	1510-1310	Five detrital wood fragments.
<u>Sandy Point:</u>						
FB06B43/43X (43-46.5 cm)	B-240534	2.28.2008	-23.8	2180±40	2320-2060	Two detrital wood fragments and 14 seeds.

* Sample code includes location identifier, year, core number, core depth in cm, subsample identifier.

** B, Beta Analytic

*** Run date, month.day.year

**** Delta 13C: 13C/12C ratio in o/oo; ND, not determined

*****Laboratory 14C age, one standard deviation

***** Calibrated age range before CE 1950, 2 standard deviations, INTCAL04

FIGURE CAPTIONS

Figure 1. A. Tectonic map modified from Wells et al. (1998) showing Oregon coast block impinging northward on the deforming Cascadia forearc. B. Northern Cascadia forearc showing known faults, mostly in southern and central Puget lowland, that accommodate Holocene-active north-south shortening. OF, Olympia fault; TF, Tacoma fault; SF, Seattle fault; SWIF, Southern Whidbey Island fault; UPF, Utsalady Point fault; DMF, Devils Mountain fault; BCF, Boulder Creek fault. C. Northwesternmost Washington and southern British Columbia showing study area bounds and ship tracks of seismic reflection data; black: commercial; red: air-gun racks (Brocher et al., 2003); blue: sparker profiles.

Figure 2. Isostatic residual gravity anomalies of the northern Cascadia forearc. Gravity data from Decade of North American Geology Bouguer gravity compilation, converted to isostatic residual anomalies using the method of Simpson et al. (1986). Black lines are selected faults. Stipple pattern indicates pre-Tertiary exposures; black areas are pre-Tertiary ultramafic rocks, including Jurassic Fidalgo Complex. White dotted lines outline gravity lows caused by sediment-filled basins. Cities: V, Vancouver; VI, Victoria; B, Bellingham; E, Everett; S, Seattle; T, Tacoma. Faults: VMF, Vedder Mt. fault; BCF, Boulder Creek fault; SJF, San Juan fault; LRF, Leech River fault; DMF, Devils Mt. fault; SWIF, southern Whidbey Island fault; SF, Seattle fault; TF, Tacoma fault. Basins: BB, Bellingham basin; EB, Everett basin; SB, Seattle basin; TB, Tacoma basin. Red dashed rectangle is area of Figures 2, 3, and 4.

Figure 3. Magnetic anomalies of the Birch Bay study area. Color contours represent total-field magnetic anomaly values measured nominally 250 m above terrain over flat areas but significantly higher over mountainous regions (Blakely et al., 1999). Magnetic anomalies reduced to pole. White lines are coastlines and lakes. Letters indicate specific anomalies discussed in text. The white area on the coast between Birch Bay and Lummi Bay is located directly over an aluminum smelter operating at the time of the survey; the intense anomaly produced by the smelter was removed from the data prior to analysis.

Figure 4. Magnetic anomalies of the Birch Bay study area filtered in order to emphasize shallow magnetic sources. Data from Figure 2 were continued upward 50 m, then subtracted from the original data. Black lines and dots indicate magnetic contacts calculated directly from magnetic data and discussed in text.

Figure 5. Interpretation of gravity and magnetic anomalies of the Birch Bay study area. Geologic map from Dragovich et al. (2002). Red dotted lines are interpreted magnetic lineaments. Black stipple indicates positive side of lineament; i.e., the uplifted side of a fault, assuming normal polarity strata. Broad dashed line is margin of Bellingham basin, as shown in Figure 1. DH, Drayton Harbor magnetic lineament; BB, Birch Bay magnetic lineament; SP, Sandy Point magnetic lineament; SF, Sumas fault; VMF, Vedder Mt. fault; BCF, Boulder Creek fault. Blue lines near Blaine are topographic scarps observed in lidar data. Yellow star at Birch Bay is location of beach-terrace inflection.

Figure 6. Map of western Whatcom county coast showing relative sea level paleoseismic study sites, core stratigraphy at selected sites, and bounds of the Lummi nation LiDAR survey. CC, Chuckanut Cove; TL, Tennant Lake; SP, Sandy Point; TC, Terrell Creek; BB, Birch Bay; DH, Drayton Harbor.

Figure 7. Drayton Harbor topographic scarp. A. Unannotated LiDAR image. B. Annotated LiDAR image showing location of topographic scarp. The topographic scarp is south-side-up and is in contrast to the channel margin erosional scarps, which are north-side-up. The south-side-up scarp is solid where observed, dashed where there is no south-side-up escarpment.

Figure 8. Ground-magnetic profiles across the Drayton Harbor scarp. Red lines indicate LiDAR scarp. Bold black lines are location of magnetic transects; positive and negative anomalies shown in red and blue, respectively, relative to an arbitrary datum. Ground-magnetic anomalies have been low-pass filtered; see text for explanation. Base map shows aeromagnetic anomalies, filtered in order to emphasize shallow sources. Black dotted lines are magnetic contacts determined directly from airborne magnetic anomalies.

Figure 9. LiDAR image in vicinity of Birch Bay showing Birch Bay and Terrell Creek paleoseismic sites. Inset showing core transects in the Terrell Creek valley bottom. Dashed line show extent of uplifted estuary and uplifted Holocene shore platform. Bold dashed line depicts best approximation of the trace of the fault, which is blind at the surface, separating Holocene subsidence (D) from Holocene uplift (U).

Figure 10. Diatom species counts from samples collected in core BB09D on the Birch Bay coastal plain (see Figure 9 for core location). Diatom flora are separated by color based on their growth environments: marine, brackish or freshwater. The core stratigraphy is interpreted based on field description of texture and color and biostratigraphic lab determination of growth environment.

Figure 11. Marine-magnetic survey and ground-magnetic transect of Birch Bay. Thin black lines show location of track and tie lines. Black dotted lines are magnetic lineaments interpreted from

aeromagnetic data. The bold black line around Birch Bay indicates the location of a ground-magnetic transect; red is positive and blue is negative relative to an arbitrary datum. White circle is southern margin of uplifted beach terrace. See Figure 5 for label definitions.

Figure 12. LiDAR image of Tennant Lake area 1.5 km south of Ferndale, Washington. LiDAR elevation data show a ca. 2 m-high scarp (red dashed line) that defines the backedge of a raised Holocene shoreline. South of the shoreline is a beach strath cut on glaciomarine drift; the strath is overlain by a thin veneer of beach sand, a paleosol and peat (see stratigraphy for cores TN-2), core is located by black dot on the image). North of the shoreline is Holocene floodplain sediment deposited by the Nooksack River.

Figure 13. A. LiDAR image of Sandy Point coastal area delineating late Pleistocene and Holocene landscapes and preserved shorelines. B. Same LiDAR image as A. but delineating a set of uplifted late Holocene shorelines (yellow, green, purple; youngest to oldest). Also shown on the Holocene platform is an abandoned, beheaded drainage and the point of stream capture. The capture was caused by headward growth of a south-flowing tributary whose gradient was increased by a drop in base level after uplift of the green shoreline. C. Topographic cross section across the modern and three paleo tide flats at Sandy Point. The red squares depict the location and elevation, within 0.5 m, of the modern shoreline angle landward of the modern tide flat and the three paleo shoreline angles for the three uplifted tide flats. Elevation of the shore line angles derived from surveying, except for the elevation of the oldest paleo shoreline angle that is approximated from the Lummi Bay 7.5' topographic map.

Figure 14. Marine sparker profile shows deformation that tentatively can be correlated to episodic coseismic uplift at Sandy Point. Correlation using aeromagnetic data shows that the same fault may be responsible for Holocene tectonic deformation (up to the northeast) at both sites. The aeromagnetic data set was processed to accentuate shallow anomalies, where dotted white lines depict steep, shallow gradients picked automatically by a gradient program. Shallow, linear anomalies that trend from onshore to offshore probably delineate geologic structure that extends to near surface or surface. The sparker profile shows Holocene sediment within 40 m of the sea floor (for location, see "Profile" on Fig. 1C). Note fold in layered sediment, which appears to be a growth fold on the flank of a bedrock ridge. The arrow on the aeromagnetic image points to the location of the fold in the sparker profile. The offset sense from the aeromagnetic and sparker profile data are consistent; the upthrown block on the profile corresponds to the magnetic strata that are nearer the surface.

Figure 15. Integration of multiple neotectonic data sets depict Holocene-active faults at, or near, the northern boundary of the Bellingham Basin

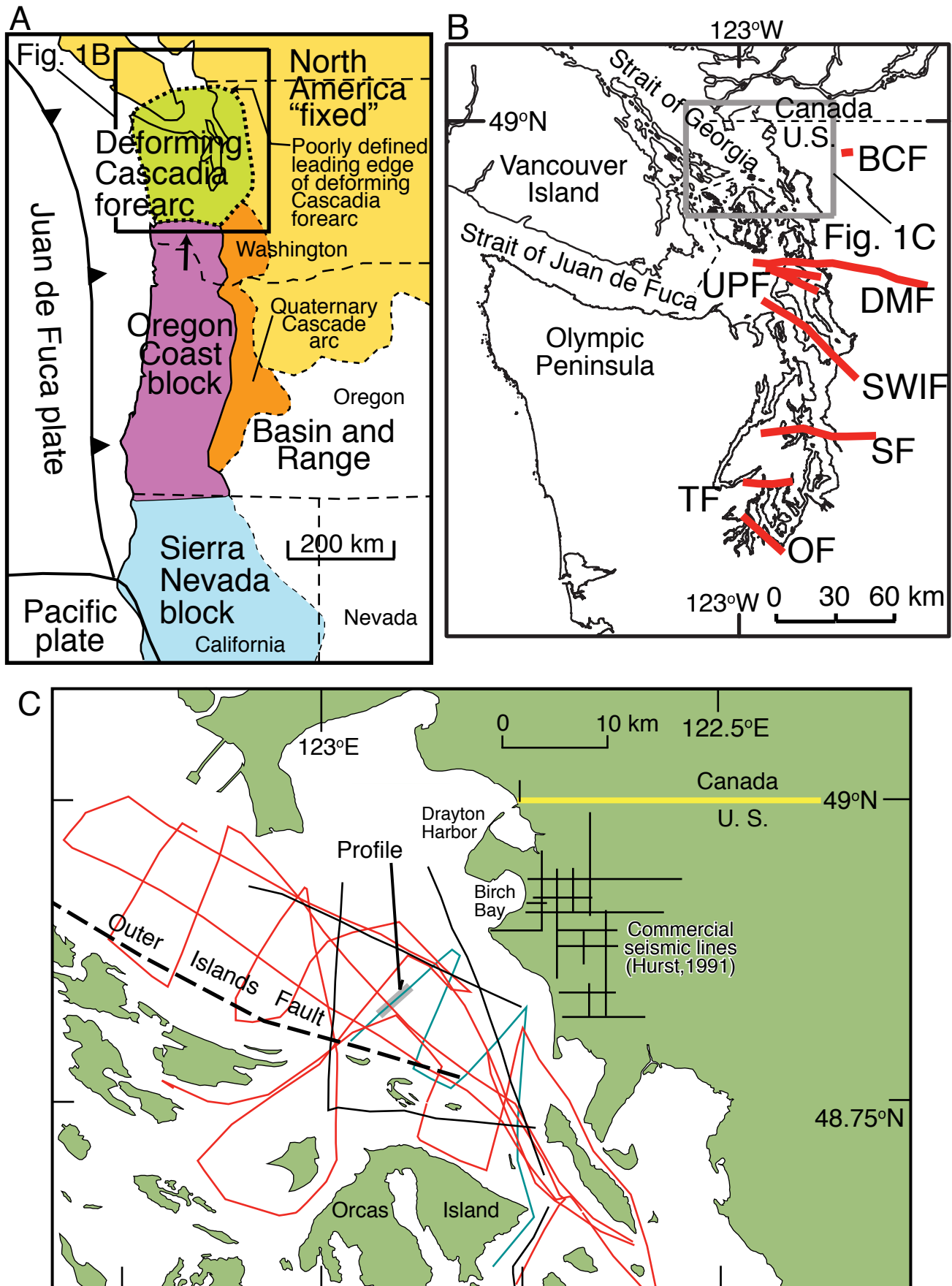


Figure 1

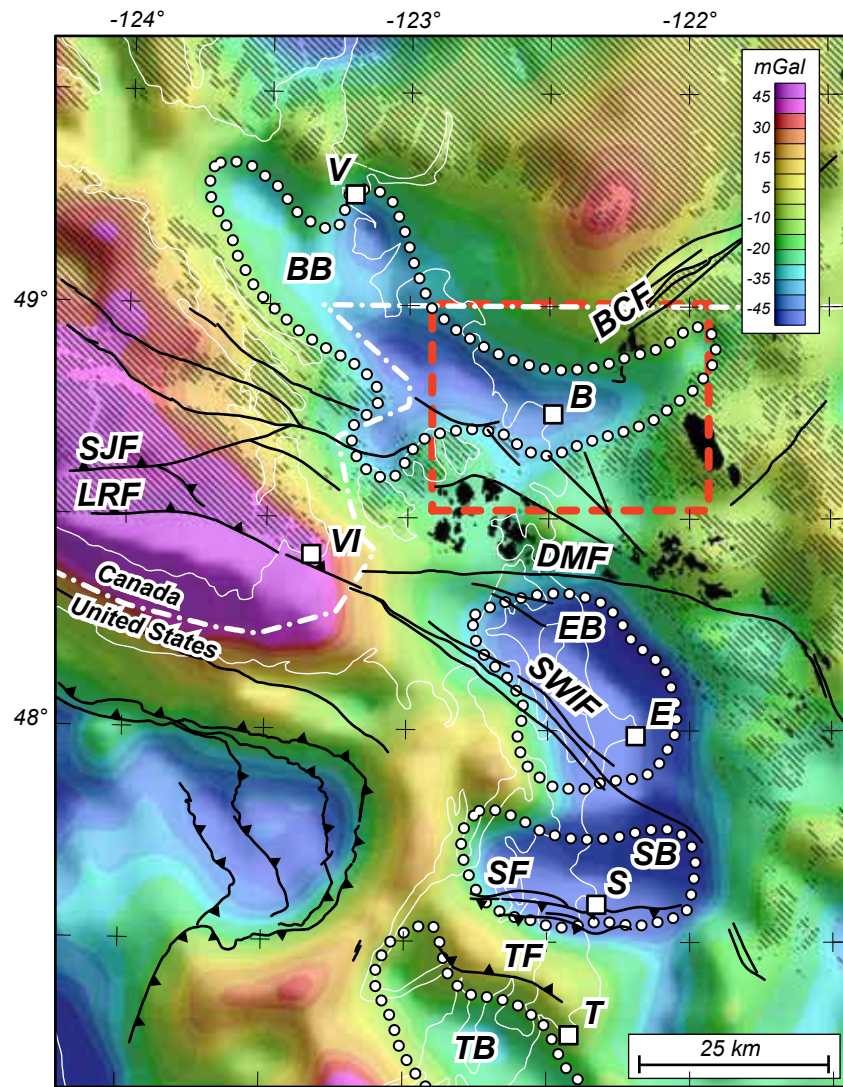


Figure 2

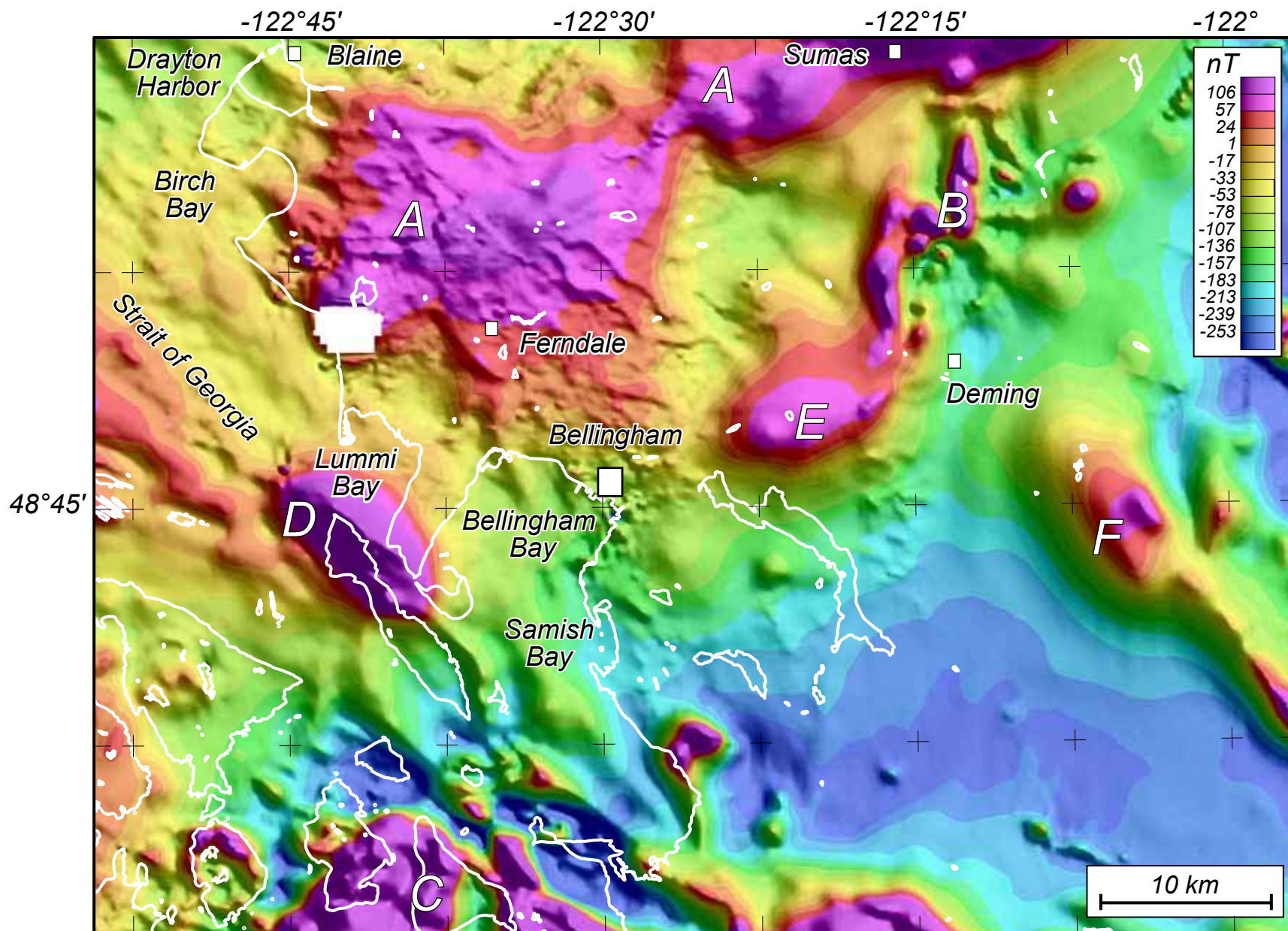


Figure 3

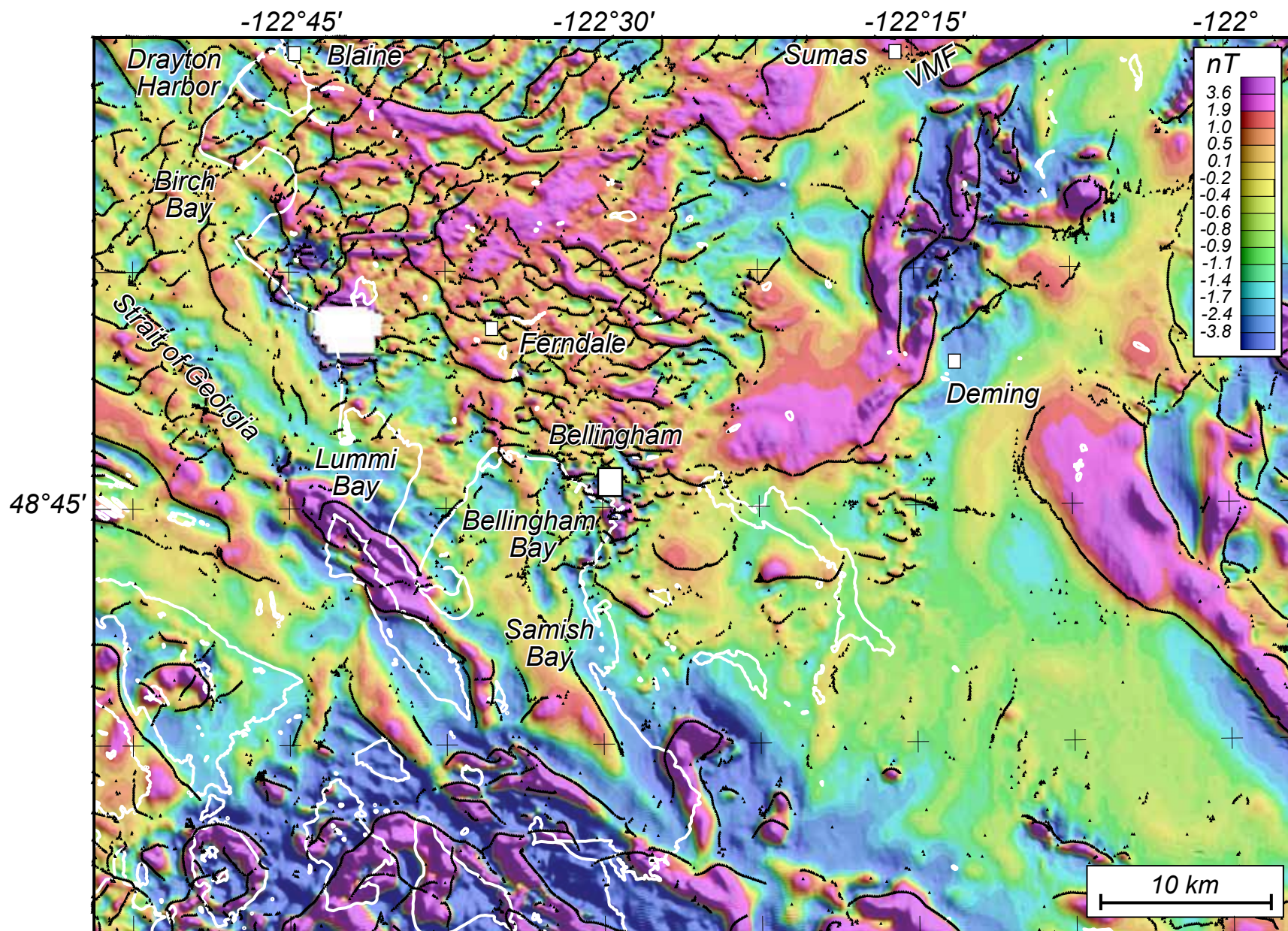


Figure 4

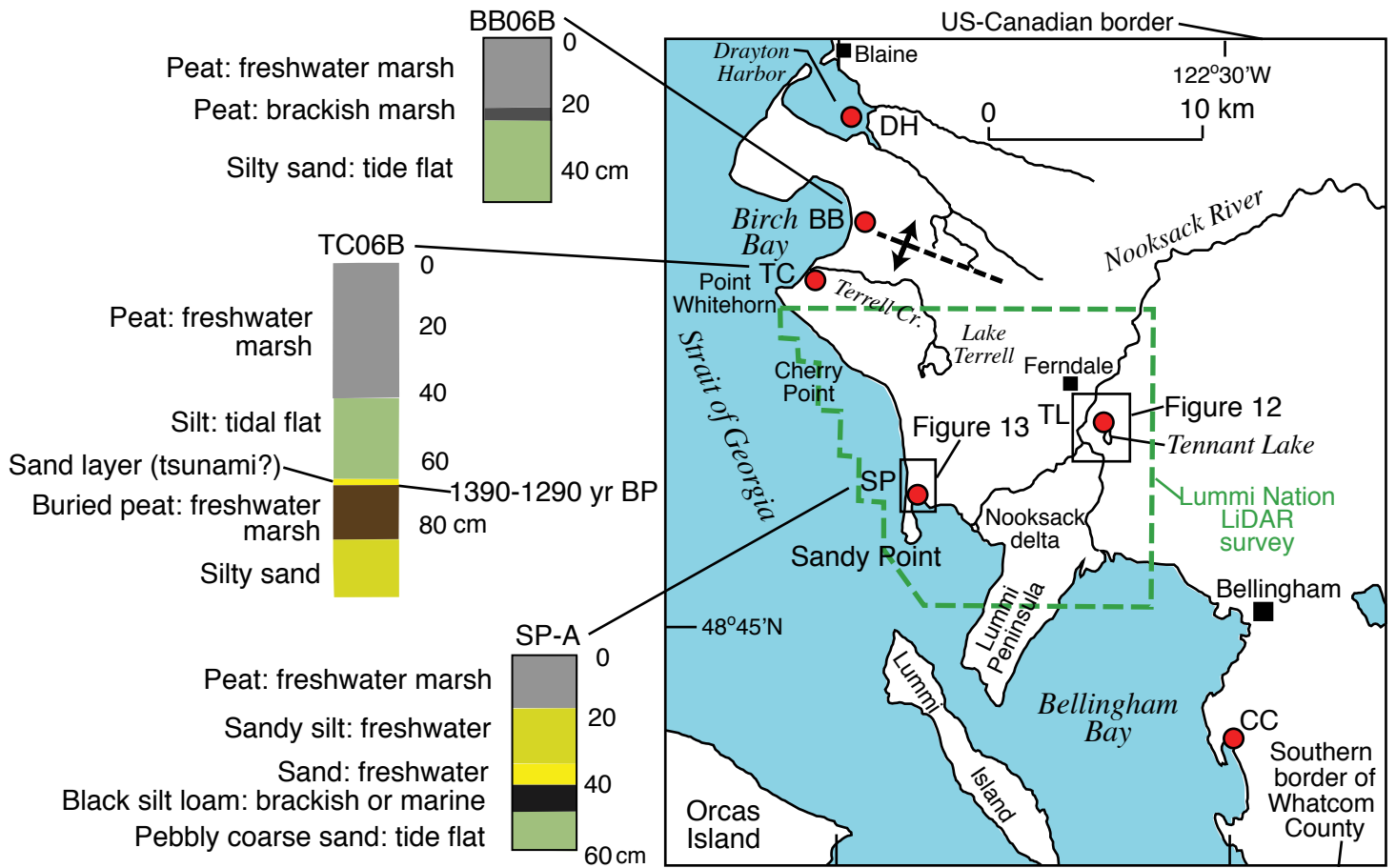
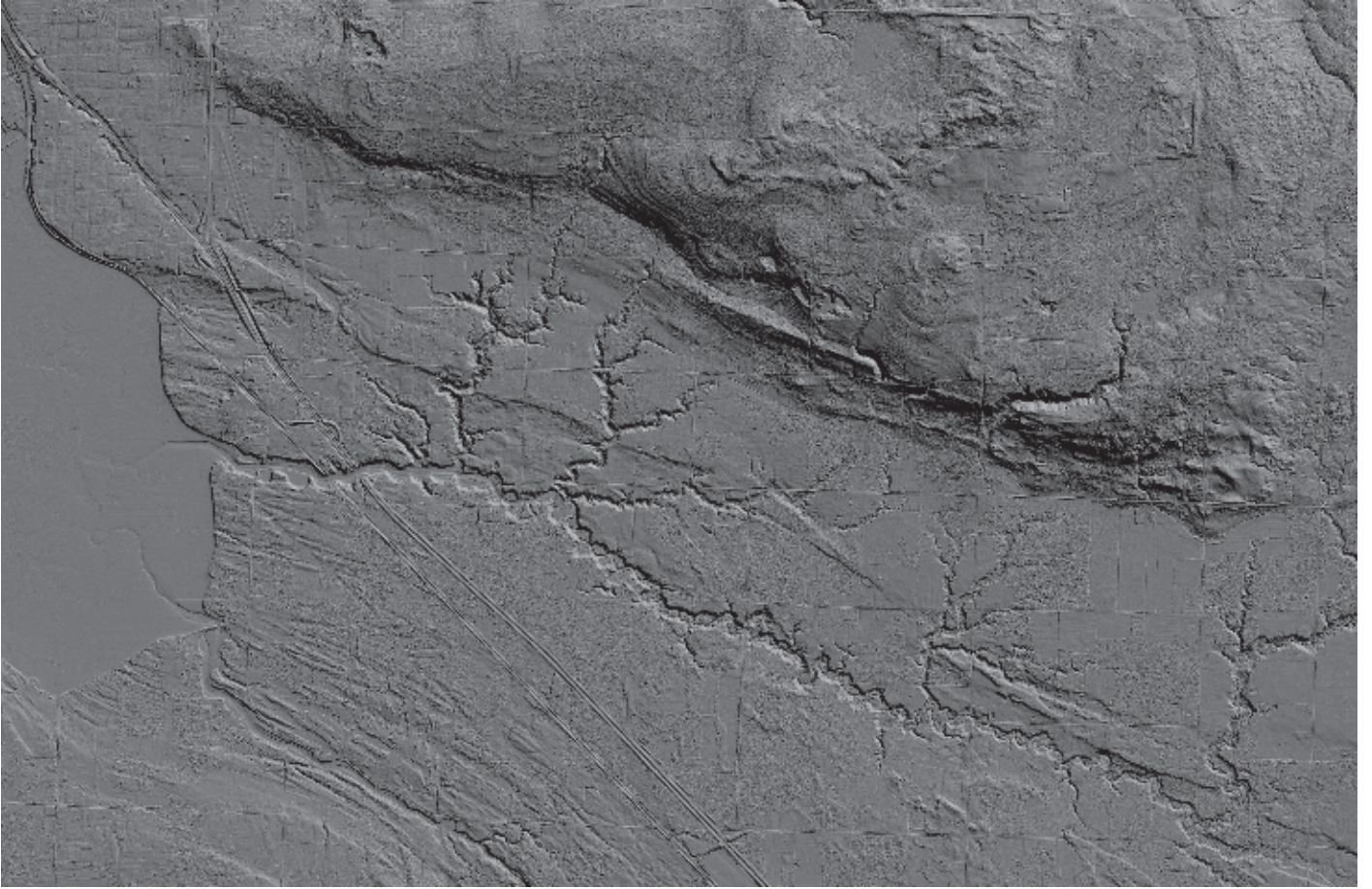


Figure 6

not annotated



annotated



Figure 7

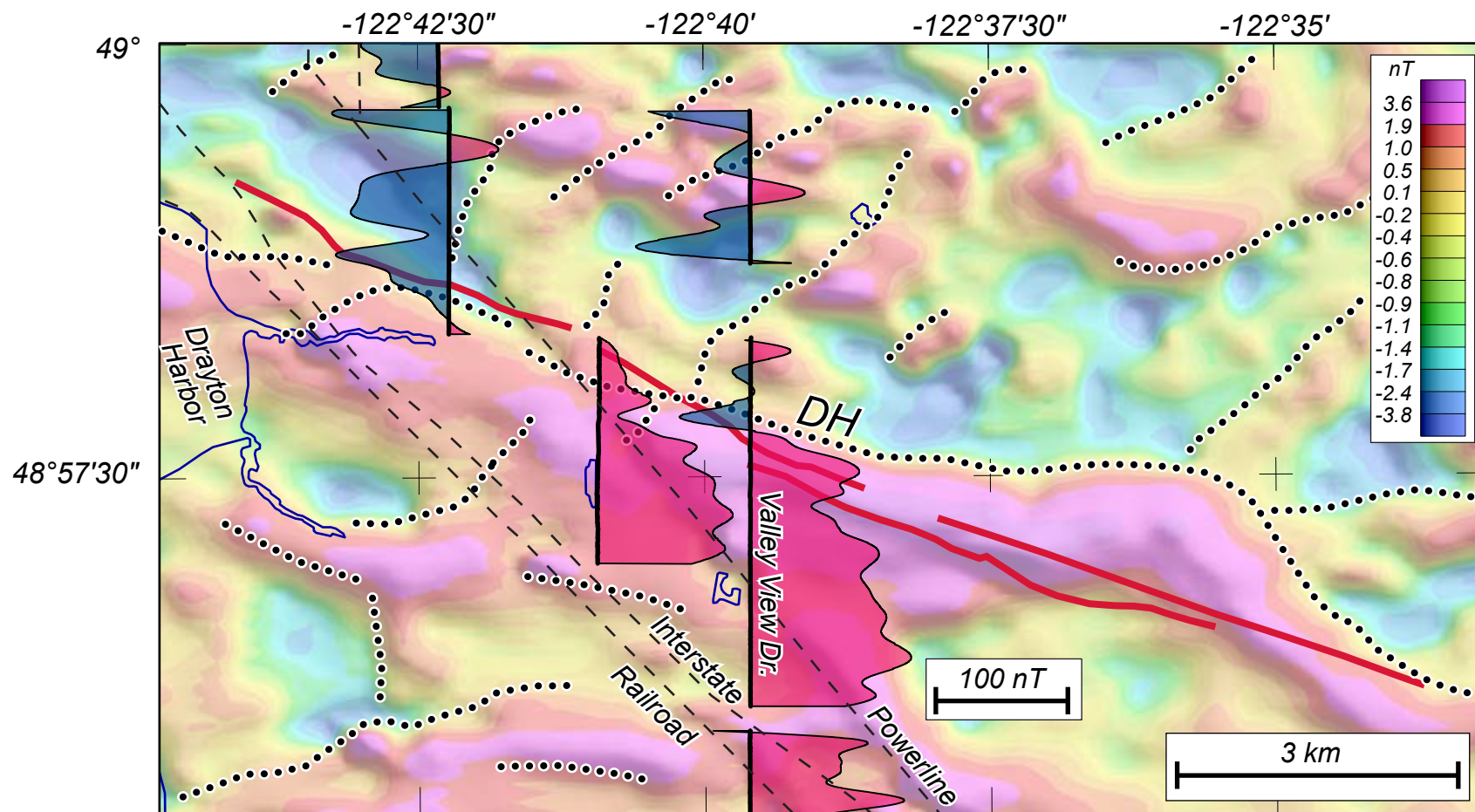


Figure 8

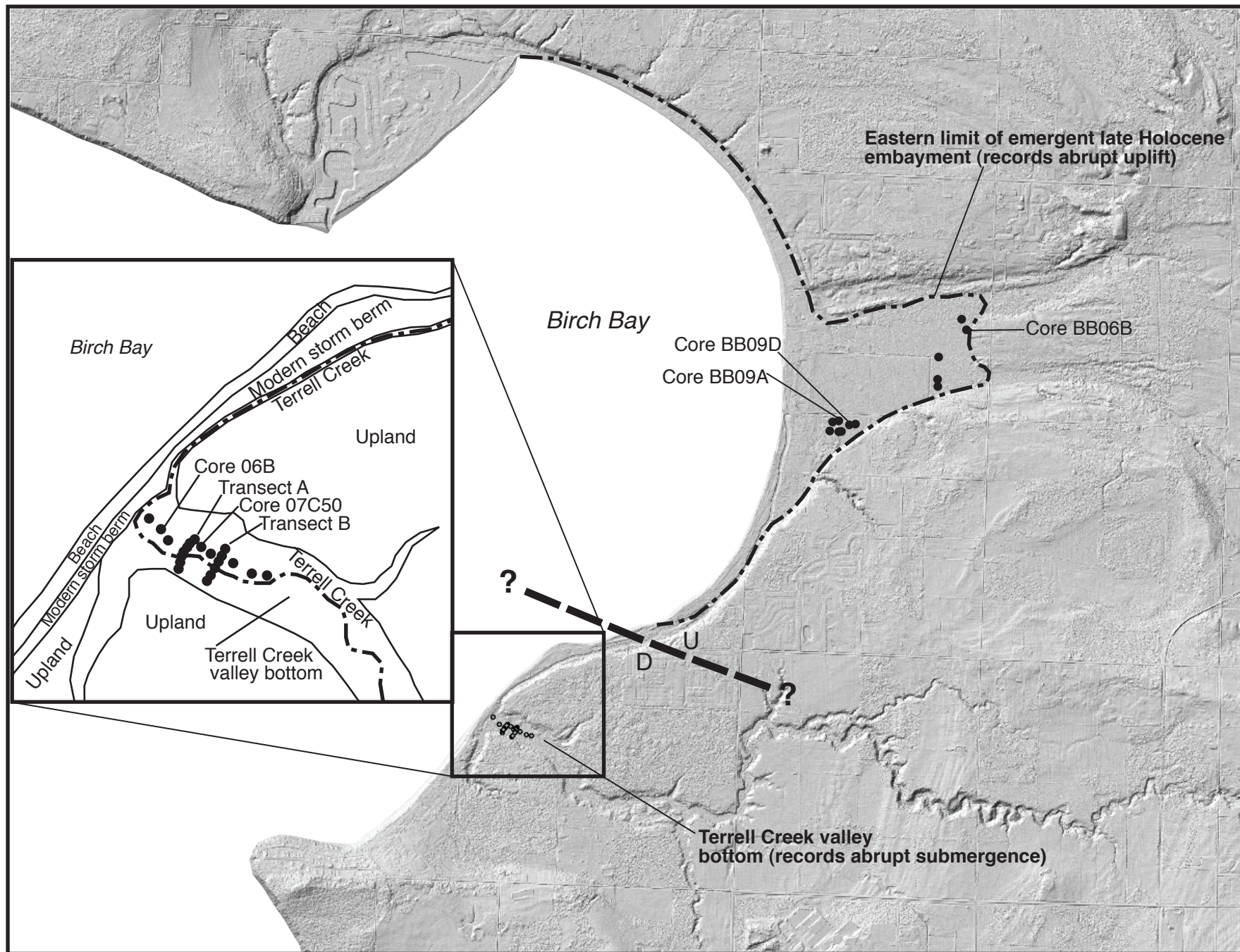


Figure 9

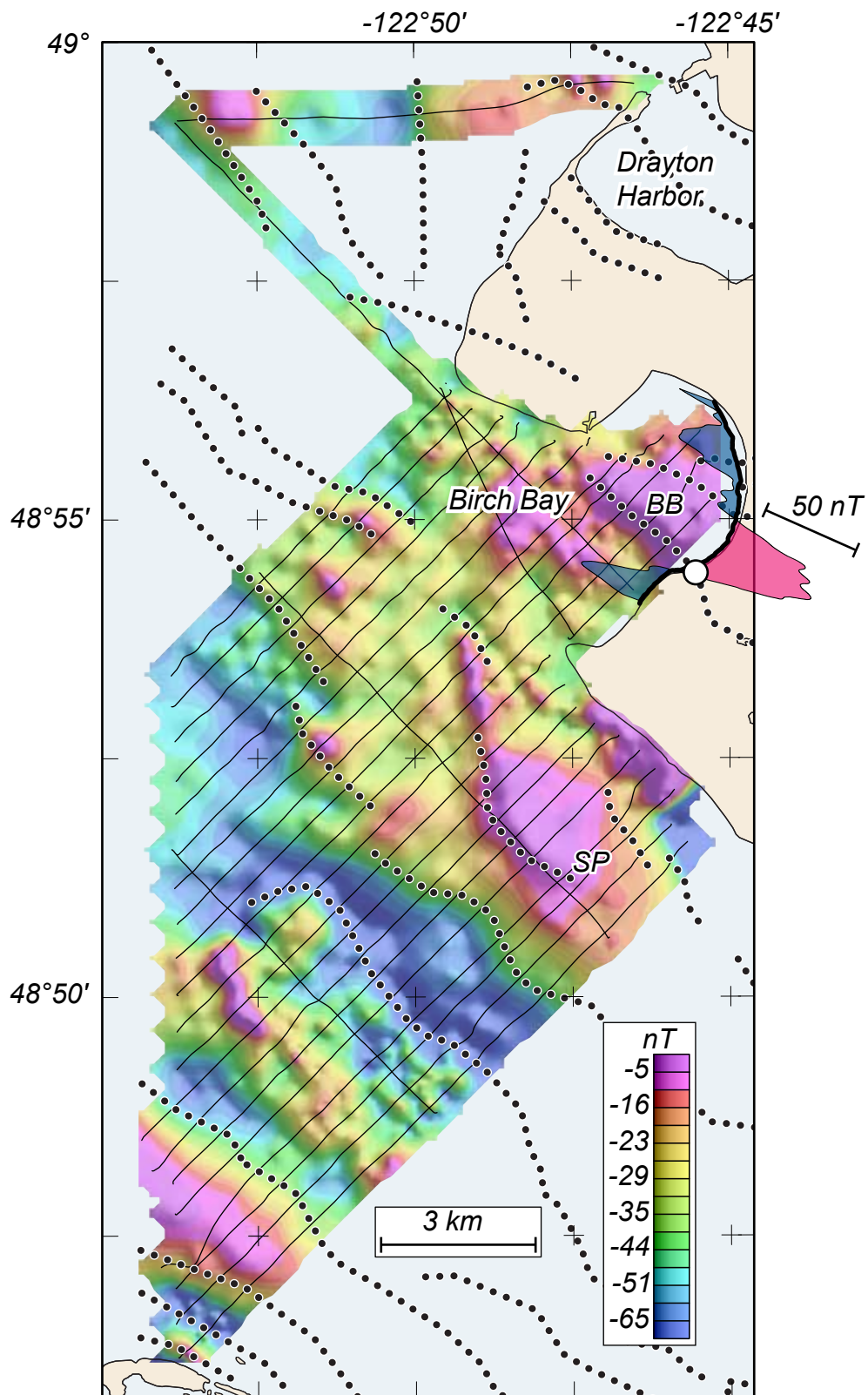


Figure 11

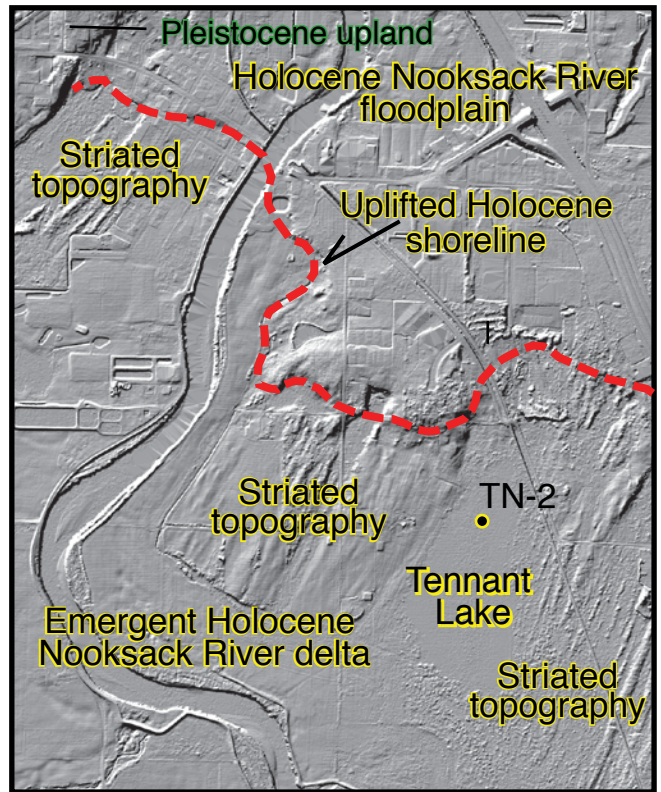
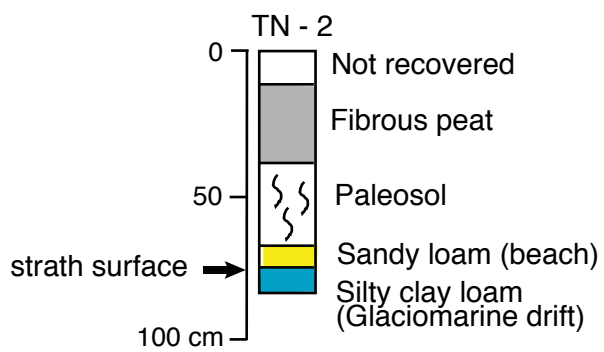


Figure 12

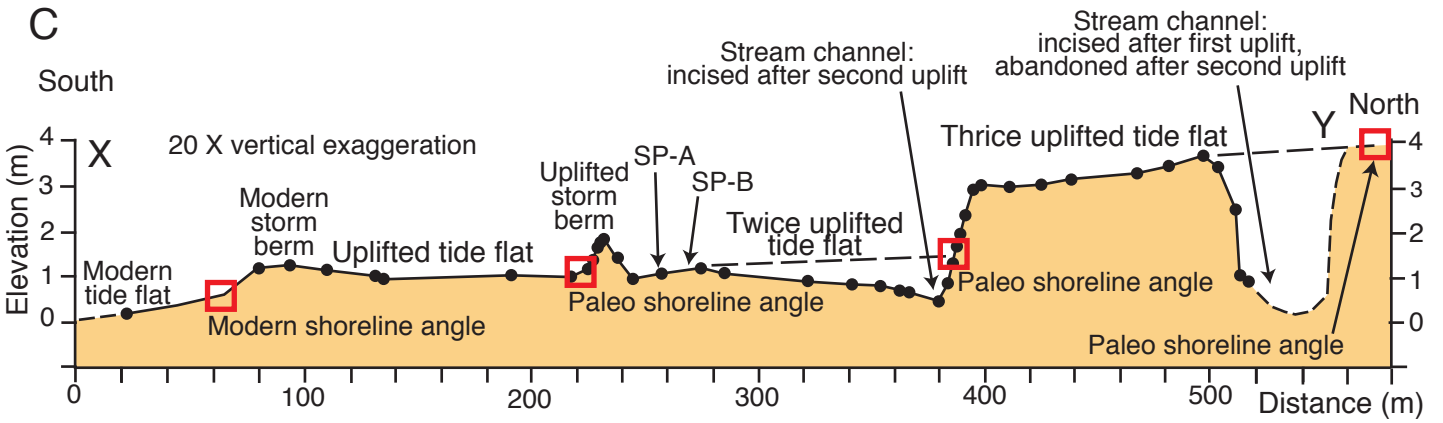
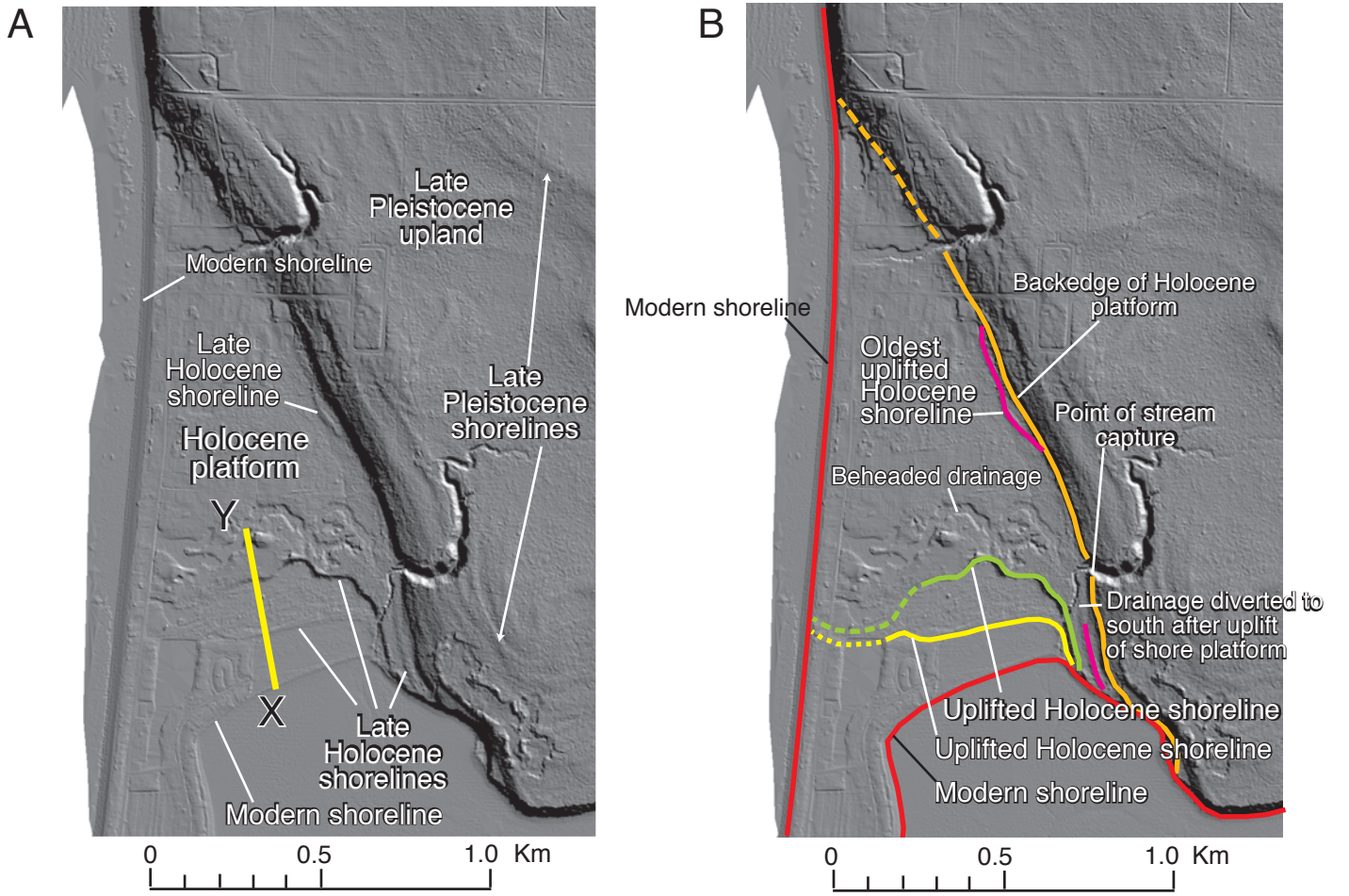
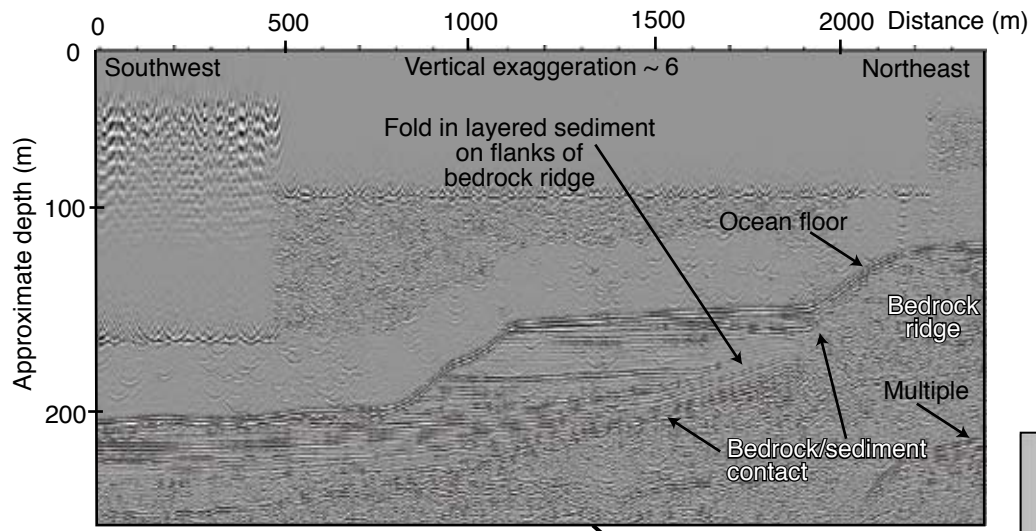


Figure 13



Sparker profile

LiDAR acquired summer, 2006 by U. S. Geological Survey

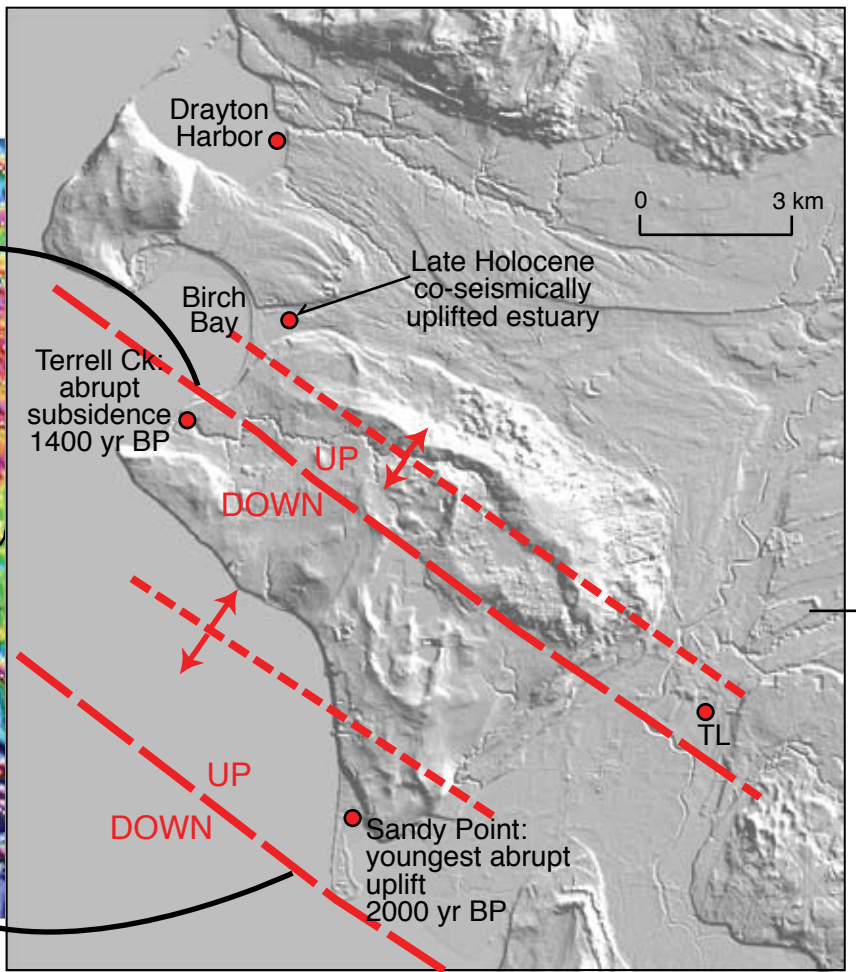
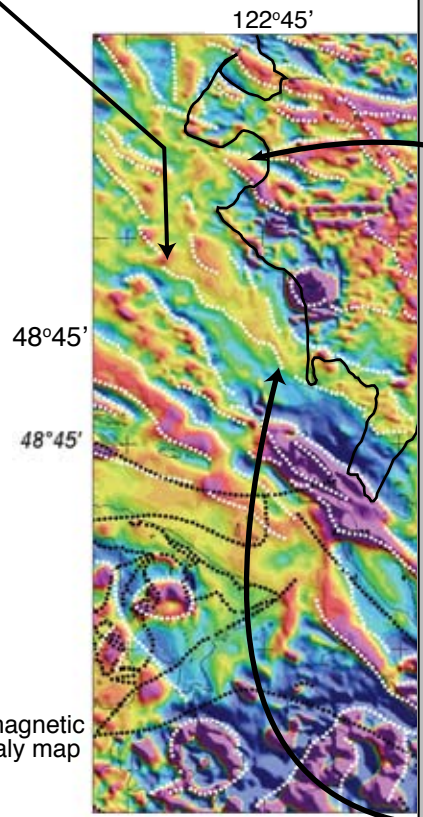
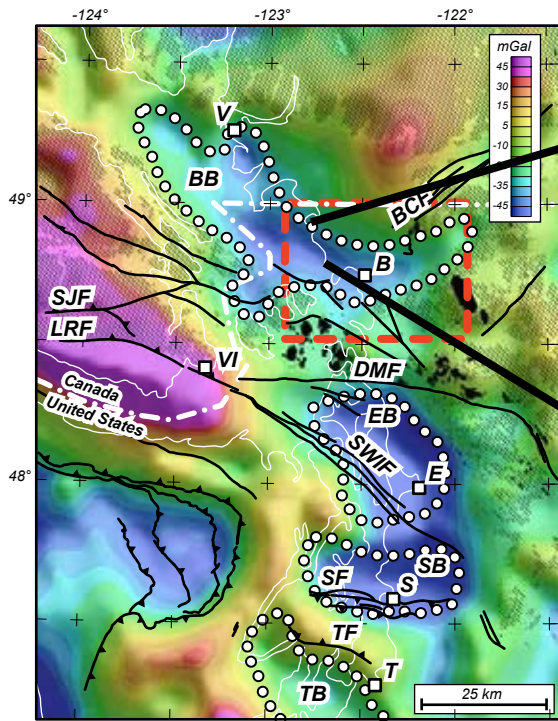
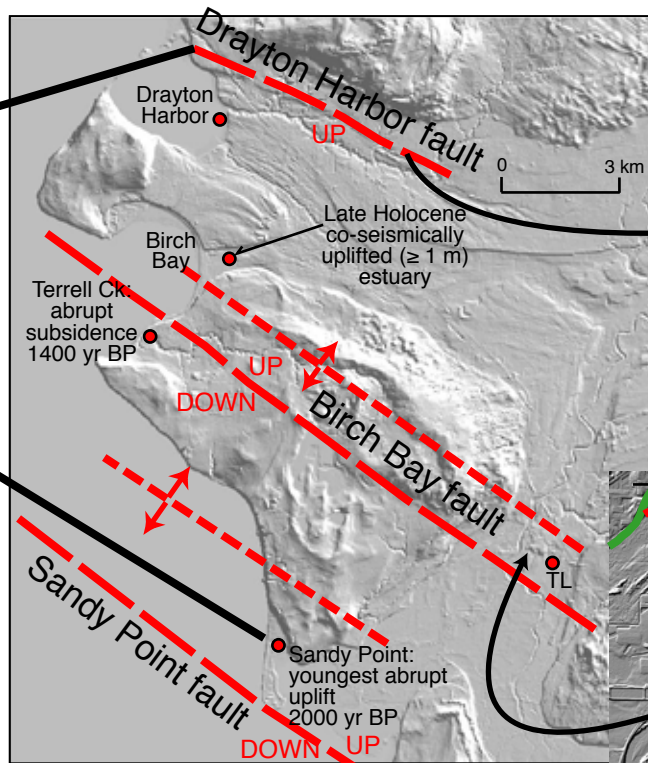


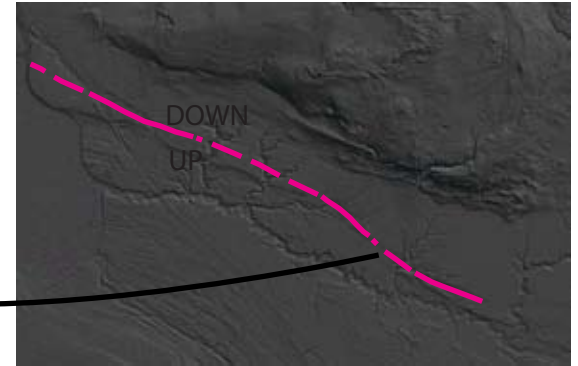
Figure 14



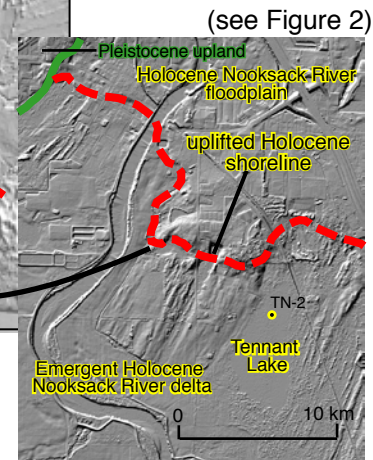
(see Figure 2)



(see Figure 14)



(see Figure 7)



(see Figure 2)

Figure 15